Current Biology

Deep evolutionary diversification of semicircular canals in archosaurs

--Manuscript Draft--

Manuscript Number:	CURRENT-BIOLOGY-D-20-01987R3
Full Title:	Deep evolutionary diversification of semicircular canals in archosaurs
Article Type:	Research Article
Corresponding Author:	Mario Bronzati, Ph.D. Faculdade de Filosofia Ciências e Letras de Ribeirao Preto - Universidade de Sao Paulo Ribeirao Preto, BRAZIL
First Author:	Mario Bronzati
Order of Authors:	Mario Bronzati
	Roger Benson
	Serjoscha Evers
	Martin Ezcurra
	Sérgio Cabreira
	Jonah Choiniere
	Kathleen Dollman
	Ariana Paulina-Carabajal
	Viktor Radermacher
	Lucio da Silva
	Gabriela Sobral
	Michelle Stocker
	Lawrence Witmer
	Max Langer
	Sterling Nesbitt
Abstract:	Living archosaurs (birds and crocodylians) have disparate locomotor strategies that evolved since their divergence ~250 million years ago. Little is known about the early evolution of the sensory structures that are coupled with these changes, mostly due to limited sampling of early fossils on key stem lineages. In particular, the morphology of the semicircular canals (SCCs) of the endosseous labyrinth has a long-hypothesized relationship with locomotion. Here, we analyze SCC shapes and sizes of living and extinct archosaurs encompassing diverse locomotor habits, including bipedal, semi-aquatic, and flying taxa. We test form-function hypotheses of the SCCs and chronicle their evolution during deep archosaurian divergences. We find that SCC shape is statistically associated with both flight and bipedalism. However, this shape variation is small and is more likely explained by changes in braincase geometry than by locomotor changes. We demonstrate high disparity of both shape and size among stem-archosaurs, and a deep divergence of SCC morphologies at the bird–crocodylian split. Stem-crocodylians exhibit diverse morphologies, including aspects also present in birds and distinct from other reptiles. Therefore, extant crocodylian SCC morphologies do not reflect retention of a ‘primitive’ reptilian condition. Key aspects of bird SCC morphology that hitherto were interpreted as flight-related, including large SCC size and enhanced sensitivity, appeared early on the bird stem-lineage in non-flying dinosaur precursors. Taken together, our results indicate a deep divergence of SCC traits at the bird–crocodylian split, and that living archosaurs evolved from an early radiation with high sensory diversity.

UNIVERSIDADE DE SÃO PAULO

FACULDADE DE FILOSOFIA, CIÊNCIAS E LETRAS DE RIBEIRÃO PRETO. DEPARTAMENTO DE BIOLOGIA.

AV. BANDEIRANTES, 3900. BAIRRO MONTE ALEGRE. RIBEIRÃO PRETO, SP. CEP 14040-901.

FAX: (16) 3602-4886

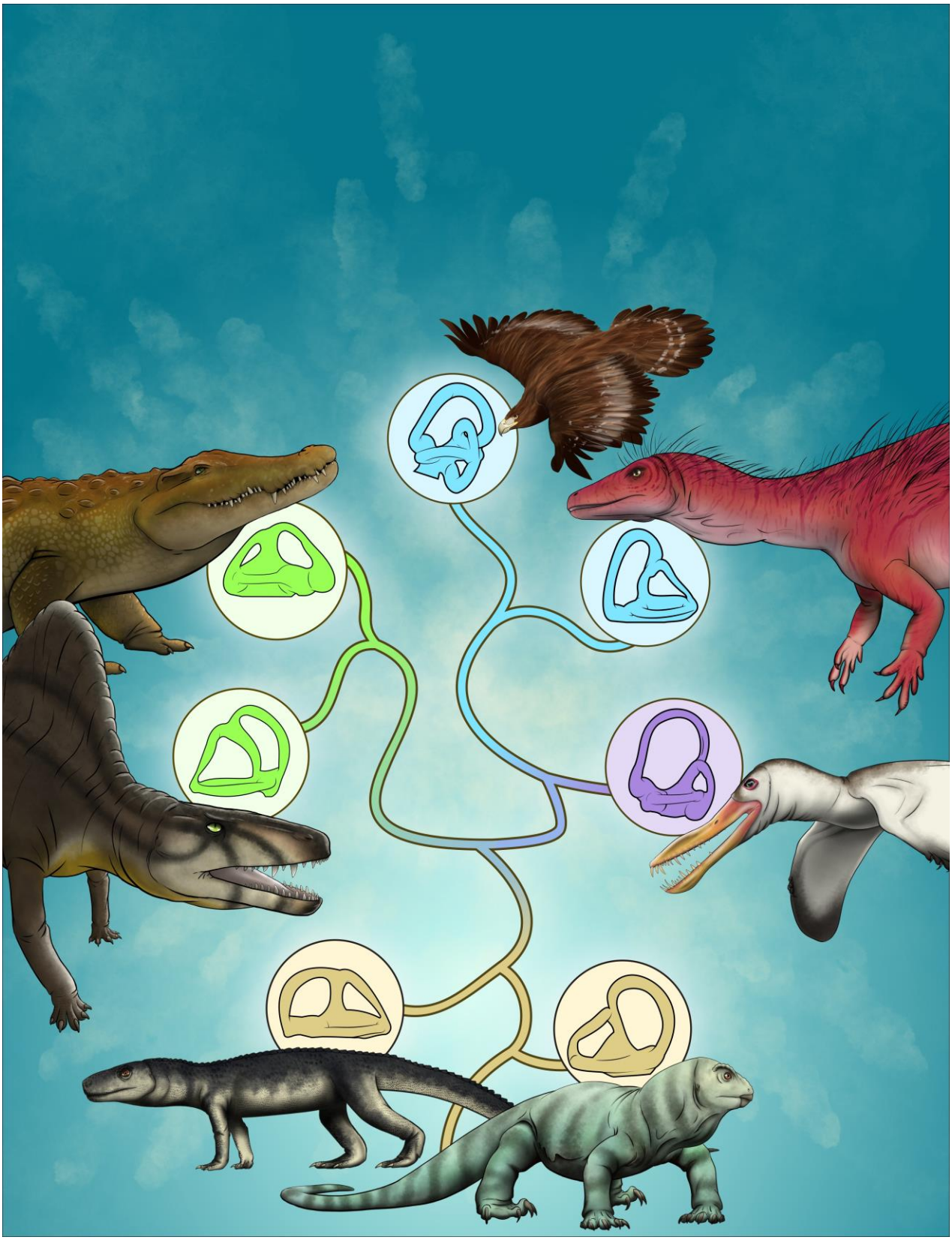

HIGHLIGHTS

> Fossils indicate a deep split in the evolution of archosaur sensory systems.

> Bird-like features of the inner ear appeared early, among non-flying dinosaurs.

> The crocodylian inner ear does not reflect ancestral reptilian or aquatic conditions.

> Variation of semicircular canal shapes is explained by spatial constraints.

IN BRIEF:

Bronzati-Benson et al. survey the semicircular canals of the inner ear, structures involved in balance control and equilibrium, in birds, crocodylians and their extinct relatives. They document great size variation among earliest fossil species, indicating a high diversity of sensory capabilities in the initial stages of the archosaur radiation.

TITLE: Deep evolutionary diversification of semicircular canals in archosaurs

Authors

Mario Bronzati[a,1,*], Roger B. J. Benson[b,c,1,*], Serjoscha W. Evers[b,d], Martín D. Ezcurra[e,f], Sergio F. Cabreira[g], Jonah Choiniere[c], Kathleen N. Dollman[c], Ariana Paulina-Carabajal[h], Viktor J. Radermacher[c], Lucio Roberto-da-Silva[i], Gabriela Sobral[j], Michelle R. Stocker[k], Lawrence M. Witmer[l], Max C. Langer[a], Sterling J. Nesbitt[k,*]

[a]Departamento de Biologia, Universidade de São Paulo, Av. Bandeirantes 1900, Ribeirão Preto-SP, 14040-091, Brazil; [b]Department of Earth Sciences, University of Oxford, South Parks Road, OX13AN, Oxford, UK; [c]Evolutionary Studies Institute, University of the Witwatersrand, Braamfontein, Private Bag 3, Johannesburg, WITS2050, South Africa; [d]Department of Geosciences, University of Fribourg, Chemin du Musée 4, CH-1700 Fribourg, Switzerland; [e]Sección Paleontología de Vertebrados, CONICET–Museo Argentino de Ciencias Naturales "Bernardino Rivadavia", Ángel Gallardo 470, C1405DJR, Buenos Aires, Argentina; [f]School of Geography, Earth and Environmental Sciences, University of Birmingham, Edgbaston, B15 2TT, Birmingham, UK; [g]Avenida Antônio Bozzetto 305, Faxinal do Soturno-RS, 97220-000, Brazil; [h]Instituto de Investigaciones en Biodiversidad y Medioambiente (INIBIOMA), CONICET-Universidad Nacional del Comahue, Quintral 1250 (8400), San Carlos de Bariloche, Argentina; [i]Rua Venâncio Trindade 810, Cachoeira do Sul-RS, 96506-290, Brazil; [j]Staatliches Museum für Naturkunde Stuttgart, Rosenstein 1, Suttgart, 70191, Germany; [k]Department of Geosciences, Virginia Tech, 926 West Campus Drive, Blacksburg, VA 24061, USA; [l]Department of Biomedical Science, Heritage College of Osteopathic Medicine, Ohio University, Athens, Ohio 45701, USA.

[1] these authors contributed equally

* Correspondence:

Lead contact: Mario Bronzati – email: mariobronzati@usp.br; TEL: +55 16 33154965;

Roger B. J. Benson – email: roger.benson@earth.ox.ac.uk, TEL: +44 1865 272076;

Sterling J. Nesbitt: sjn2104@vt.edu, Tel: +1 540 231 6330.

Twitter handle: @BronzatiMario , @BensonLabOxford , @VTechmeetsPaleo

SUMMARY

Living archosaurs (birds and crocodylians) have disparate locomotor strategies that evolved since their divergence ~250 million years ago. Little is known about the early evolution of the sensory structures that are coupled with these changes, mostly due to limited sampling of early fossils on key stem lineages. In particular, the morphology of the semicircular canals (SCCs) of the endosseous labyrinth has a long-hypothesized relationship with locomotion. Here, we analyze SCC shapes and sizes of living and extinct archosaurs encompassing diverse locomotor habits, including bipedal, semi-aquatic, and flying taxa. We test form-function hypotheses of the SCCs and chronicle their evolution during deep archosaurian divergences. We find that SCC shape is statistically associated with both flight and bipedalism. However, this shape variation is small and is more likely explained by changes in braincase geometry than by locomotor changes. We demonstrate high disparity of both shape and size among stem-archosaurs, and a deep divergence of SCC morphologies at the bird–crocodylian split. Stem-crocodylians exhibit diverse morphologies, including aspects also present in birds and distinct from other reptiles. Therefore, extant crocodylian SCC morphologies do not reflect retention of a 'primitive' reptilian condition. Key aspects of bird SCC morphology that hitherto were interpreted as flight-related, including large SCC size and enhanced sensitivity, appeared early on the bird stem-lineage in non-flying dinosaur precursors. Taken together, our results indicate a deep divergence of SCC traits at the bird–crocodylian split, and that living archosaurs evolved from an early radiation with high sensory diversity.

Keywords

Semicircular canals; sensory system; locomotion; archosaurs; extinct; living; birds; crocodylians; dinosaurs; pterosaurs.

INTRODUCTION

Birds and crocodylians represent Archosauria today, and the rich evolutionary history of archosaurs is documented by the fossil record of extinct groups such as dinosaurs and pterosaurs on the avian-line (= Avemetatarsalia, Pan-Aves) and phytosaurs and rauisuchids on the crocodylian-line (= Pseudosuchia, Pan-Crocodylia). These two major lineages (Figure 1) diverged nearly 250 million years ago, and their living members have contrasting ecologies [1]. Most birds are active bipedal fliers, whereas crocodylians are semiaquatic quadrupeds [2,3]. The oldest archosaurs date back to the aftermath of the Permian/Triassic mass extinction (*ca* 249 Ma), and archosaur stem-lineage extends still farther back in time (*ca* 256 Ma) [4]. Stem-archosaurs were ancestrally terrestrial or semi-aquatic quadrupeds with sprawling limb orientations [5]. Their descendants diversified rapidly from this ancestral body plan, repeatedly evolving more erect limb postures, flight, obligate aquatic habits and active lifestyles [6-9], achieving incredible ecological disparity. Their locomotor diversity has been explored in detail

based on limb anatomy [6-12], and ultimately must also be linked to transformations in the sensory systems that facilitate locomotion [13]. However, these changes, and their evolutionary implications, have been poorly explored so far.

Sensory information on head rotation derives from the semicircular canals (SCCs) of the inner ear, or 'labyrinth'. These canals play an important role in the coordination of balance and navigation during locomotion, and also helps coordinating the vestibulocollic (VCR) and vestibulo-ocular (VOR) reflexes. These reflexes facilitate locomotion by driving compensatory movements of the eyes, head, and neck to stabilize the image on the retina within the visual field [14-17]. SCC morphology has been investigated in reptiles [18-22], but more extensively in mammals (e.g. [23-28]), and has hypothesized functional relationships with locomotor style, agility, and visual acuity. For example, the sizes of the SCCs, represented in previous studies by various parameters, including their duct lengths, radius of curvature, and centroid size, may be related to agility [24,29,30] or visual acuity [27] in mammals. Likewise, the reportedly large SCCs of birds, which enhance their functional sensitivity, are hypothesized to be related to their status as agile, flying animals [21,31]. Other aspects of morphological variation, including canal circularities, orthogonality and aspect ratios also have hypothesized links to locomotor style (e.g., [20,26,28,32,33]). Nevertheless, strict form-function relationships of the SCCs are poorly supported by comparative phylogenetic analyses and in studies at broad phylogenetic scales (e.g., [20,21,34,35]).

Crocodylians have angular canals, with a low, broad aspect ratio similar to those of other extant groups of non-avian reptiles — lepidosaurs and turtles [36]. In contrast, birds exhibit more rounded canals, with a high aspect ratio, and a ventrally-displaced posterior canal [21,36]. These divergent morphologies have hypothesized, but as-yet untested, relationships to differences in the structure, ecology or locomotion of living archosaurs. Moreover, the rich fossil record of early archosaurs and their stem-lineage documents a wide range of locomotor strategies not represented among extant members of the group [37]. However, the potential of these fossils to test hypotheses of the drivers of variation in SCCs morphology has not yet been realized.

Using computed tomographic (CT) scans, we compiled a dataset of 3D virtual models of the semicircular canals of 83 extinct and extant reptiles, focusing on archosaurs (Supplemental Information). Previous studies proposed form-function associations between SCC geometry and locomotion in archosaurian subgroups based primarily on qualitative evidence [18, 32]. Here, we used 3D geometric morphometrics and phylogenetic comparative analyses to statistically test these associations. Our taxon sample includes members of all major groups of extant reptiles and fossils representing most of the stem-archosaur clades, and the earliest members of different subgroups of both the crocodylian and avian lineages for which information is available (e.g. [38-42]).

RESULTS

Our principal components analyses (PCA) describe major aspects of SCCs shape variation among extant reptiles (including birds) and extinct archosauromorphs (= archosaurs + stem archosaurs; pan-archosaurs) (Figure 2). Principal component one (PC1) describes large shape differences between the SCCs of birds (positive values) and extant non-avian reptiles (mainly negative values), encompassing more than half the shape variation in our dataset (57.6% [full analysis]; 47.0% [reduced analysis] – see Methods). Positive (bird-like) values of PC1 indicate a more orthogonal arrangement of canals, which are individually more circular (Supplemental Information – Data S1G). In birds, the posterior semicircular canal (PSC) extends ventral to the lateral semicircular canal (LSC), and the anterior semicircular canal (ASC) is greatly lengthened, extending posterodorsally beyond the PSC to form a prominent loop (Figures 1-3; Figures S3 and S5). This is unlike the geometry of the SCCs in other extant reptiles, in which the ASC does not extend posterodorsally to the PSC, and the ventralmost part of the PSC is housed together with the LSC within a shared endosseous recess (Figures 1-3).

Principal component two (PC2) describes differences between many extinct archosauromorphs (Figure 2), especially dinosaurs and some pseudosuchians (positive values) from both birds and other extant reptiles (mainly negative values), encompassing 11.1% of shape variation (or 12.7%, reduced dataset). Positive values of PC2 correspond to labyrinths with more orthogonal SCCs (Supplemental Information – Data S1G), a mediolaterally narrower LSC, and a dorsoventrally tall, anteroposteriorly narrow ASC compared to the PSC (Supplemental Information - Figures S3 and S5). Subsequent principal component axes describe less variation and are not highly structured with respect to archosauromorph evolution (Figures S2 and S4).

Our PCA results show that extinct archosauromorphs occupy a different morphospace to those of living birds or crocodylians. Surprisingly, few extinct archosauromorphs show labyrinth geometries similar to those of crocodylians or other non-avian reptiles. Extinct pseudosuchians exhibit a higher disparity of labyrinth shape than that of crocodylians (Procrustes variance = 0.007 in Crocodylia compared to 0.011 in their stem lineage; $p_{permutation}$ = 0.001), including morphologies that share some limited shape aspects with those of birds (Figure 2 and Supplemental Information). Dinosaurs share still more shape aspects with birds, including a longer ASC, more orthogonal canals and taller common crus, occupying an intermediate region of morphospace that is distinct from most pseudosuchians. A particularly bird-like morphology is present in *Velociraptor,* a close evolutionary relative of birds (Figure 2). Nevertheless, some pterosaurs, non-dinosaurian avemetatarsalians (*Dromomeron*, *Ixalerpeton*), and stem-archosaurs (*Trilophosaurus*, *Triopticus*) also possess bird-like SCCs, more so than the early (Triassic–Early Jurassic) non-avian dinosaurs from our sample (Figure 2 and Supplemental Information).

Procrustes distance-based phylogenetic regression demonstrates prominent allometric variation in labyrinth shape (Table 1). Allometric shape variation is represented by the size-related explanatory variables skull length, postrostral skull length, and labyrinth centroid size, which yielded significant p-values in many of the models in which they are included (Table 1).

An interaction term 'postrostral skull length:labyrinth centroid size' is consistently found to be statistically significant and describes a situation in which the effects of variation in labyrinth size depends on skull size. Size-related shape deformations indicate an effect in which taxa with proportionally large labyrinths have more circular canals that are more orthogonal to each other (Figure 3 and Supplemental Information - Data S1G).

Several locomotor traits (see Supplemental Information – Table S1) have significant, independent effects on labyrinth shape: bipedal | quadrupedal gait, semi-erect | erect limb postures, and flying | non-flying locomotion (Table 1). The effects of bipedality and erect limb postures are statistically redundant with one another, being individually significant (Table 1), but having non-significant partial effects when analyzed together (Supplemental Information - Data S1A). Their coefficients indicate that the evolution of bipedality and/or erect stances correlates with an increase in the relative height of the ASC and common crus, and with increases in the orthogonality (Supplemental Information - Data S1G). The evolution of flight correlates with an increase in the circularity of the ASC, and with posterodorsal extension of the ASC relative to the PSC and LSC. These effects are independent from those of relative labyrinth size and all coefficients are statistically significant when included together in the same model (i.e. shape ~ postrostral length:labyrinth centroid size + bipedality [or erect limb postures] + flight; Table 1). However, these represent relatively small changes that individually explain approximately 5% of total shape variation (Table 1).

Aquatic habits do not provide a statistically-significant explanation of labyrinth shape variation in any of the models evaluated (Supplemental Information – Data S1A), or when pseudosuchians, avemetatarsalians or non-avemetatarsalian archosauromorphs are analyzed individually (Supplemental Information – Data S1B-D). The height/width aspect ratio of the posterior part of the skull is non-significant in all models describing labyrinth shape variation among archosauromorphs. However, it is strongly significant and highly predictive, explaining up to 26% of shape variation, when pseudosuchians or non-avemetatarsalian archosauromorphs are analyzed separately (Supplemental Information – Data S1B-D).

Phylogenetic generalized least squares regressions find strong evidence of a correlation between labyrinth size (i.e., centroid size) and either skull length or postrostral skull length, with clear negative allometry (Tables 2-3; coefficients << 1.0). This is found for both smaller sample sizes (N = 52 species; for which all size and most locomotor traits are known; see methods; Data S1E) and larger sample sizes (N = 57; for which only all size traits are known; Table 2). A relationship of labyrinth size to postrostral skull length is consistently favored over a relation to overall skull length by Akaike weights, suggesting that variation in rostral length does not influence labyrinth size. Locomotor traits are not significant on their own as explanations of absolute labyrinth size variation and such models have negligible AICc weights (Supplemental Information - Data S1E-F). Nevertheless, we find weak evidence that the evolution of erect limb postures (present in dinosaurs and some pseudosuchians such as *Arizonasaurus* and *Saurosuchus*; see Supplemental Information -Table S1) or bipedal gait (present in dinosaurs and the pseudosuchian *Postosuchus*) is linked to an increase in relative labyrinth size (i.e. when

analyzed alongside head size variables; Tables 2-3). The categorical variables describing these locomotor traits have statistically significant p-values in our analyses (Supplemental Information - Data S1E-F). However, models including these variables receive less support from AICc than models that exclude them, suggesting that more evidence is needed to definitively establish their importance.

The residuals from a regression of labyrinth size on postrostral skull length indicate differences between labyrinth size and expectations based on scaling relationships. These show a general pattern in which avemetatarsalians, including early representatives such as non-avian dinosauromorphs, have proportionally large labyrinths (Figure 4 and Supplemental Information) similar to those of birds (t test; bird mean = 0.081; non-avian avemetatarsalian mean = 0.119; df = 29.0; $p = 0.12^{NS}$). The average labyrinth size of avemetatarsalians is 32% greater than that of stem-archosaurs, whereas pseudosuchians show an overall increase of only 17% compared to stem-archosaurs. Nevertheless, avemetatarsalians, including both birds and non-avian taxa, encompass a wide range of relative labyrinth sizes, with some species having similar relative labyrinth sizes to those of crocodylians (Figure 4; Figure S8A).

DISCUSSION

We found considerable and unexpected variation in SCC morphologies among extinct archosauromorphs, including distinctive morphologies that are not found among living reptiles. Early archosauromorphs show large variation in SCC size, comparable to that seen among extant archosaurs, indicating substantial variation in their locomotor-related sensory capabilities (Figures 1-3). We find a particular increase in relative size of the labyrinth occurring early on the bird stem-lineage (Figure 4). We also find a positive association between relative size of the SCCs and increases in canal circularity (Figure 3; Supplemental Information - Data S1G), an association that may reflect either functional optimization or an influence of braincase architecture on SCC shape with increasing relative labyrinth size [21,33]. Changes in SCC geometry are also associated with key locomotor shifts, such as the origins of flight, and bipedal or erect limb postures. However, these associations explain only a small fraction of overall shape variation, representing an even smaller fraction of functional variation given that shape variation has relatively little impact on SCC sensitivity compared to the effect of size variation [43,44].

Testing ecomorphological adaptations of the archosaur labyrinth

Flight evolved independently in two archosaur groups, first in pterosaurs [7] and later in paravians, a group of long-armed theropod dinosaurs that also includes birds [45]. Our analyses recover shared traits of the bird and pterosaur SCCs as statistically associated with flight. These include the acquisition of more orthogonal canal arrangements and increases in their circularities, and lengthening of the ASC, which extends further posterodorsally (Figure 3). These shape changes deserve functional analysis to evaluate their relationship to the hypothesized requirement for agile locomotion involved in flight. However, non-functional

explanations may be more likely, such as constraints imposed on morphology of the ASC due to enlargement of the floccular lobe in pterosaurs [18] and some birds (e.g. [46]), or by other possible shared traits of their braincase morphologies such as anteroventral rotation of the craniocervical articulation [18].

We reject the generally accepted hypothesis that vertebrate flight entails an increase in the proportional size of the labyrinth to enhance sensitivity [47]. Instead, flying birds exhibit similar labyrinth sizes to those of non-flying avemetatarsalians in our dataset (Figure 4 and Supplemental Information). Furthermore, the flightless bird *Casuarius casuarius* possesses one of the largest labyrinths in our dataset (Figure 4), and there is no evidence for reduced labyrinth sizes in other flightless birds compared to their flying relatives [21]. We also show that pterosaurs have reduced or intermediate relative SCC sizes when compared to non-flying archosauromorphs (Figure 4 and Supplemental Information), contrary to qualitative descriptions of large SCCs compared to brain size in pterosaurs [18]. This is similar to the condition in bats, flying mammals that have relative SCC sizes similar to those of other small-bodied mammals [48], substantially undermining the hypothesized link between labyrinth size and flight.

The proportionally largest SCCs of extant species in our dataset seen in birds, including raptors and other visual specialists (see also [21]). We therefore suggest that the large SCCs of some flightless non-avian avemetatarsalians may be explained by enhanced visual acuity resulting in a higher demand for precise gaze stabilization, as found in mammals (e.g. [27]) and suggested for birds [21]. Alternatively, large labyrinths in non-flying dinosauromorphs might be related to the evolution of more agile/cursorial locomotion [12, 24, but see 27]. This theoretical locomotor “superiority” compared to other archosaurs has been suggested as an explanation for the evolutionary success of dinosaurs in Mesozoic ecosystems [6,49].

We find no evidence for changes in labyrinth shape associated with transitions to aquatic or semiaquatic habits, either across archosauromorphs, in non-avemetatarsalian archosauromorphs, or in Pseudosuchia (Supplemental Information - Data S1C-D). This contrasts with previous studies that reported both dorsoventrally low aspect ratios in the SCCs of aquatic taxa [32,50,51] and an increase in endosseous canal diameters during the early stages of aquatic adaptation [51] but did not include phylogenetically informed statistical tests of those hypotheses. Instead, we show an association between labyrinth shape and the height/width aspect ratio of the postrostral part of the skull in pseudosuchians and in non-avemetatarsalian archosaurs more broadly (Data S1C-D). This suggests that the dorsoventrally low labyrinth of some aquatic reptiles [32] is in fact explained by the low, broad skulls of those taxa.

Overall, our analyses show that SCC shape has less predictive value than expected for inferring locomotory traits. At most, only 10.7% of evolutionary shape variation in archosaur labyrinths is potentially attributable to the first-order locomotory traits that we analyzed (flight, bipedality or erect limb orientations; Table 1). This leaves substantial unexplained variation, some of which is accounted for by spatial constraints imposed by skull geometry: absolute and relative allometric effects explain up to 14.4% of evolutionary shape variation. Although

pterosaurs and birds share specific aspects of SCC morphology, overall SCC geometries of pterosaurs are not especially closer to those of flying birds than are those of some non-flying dinosauromorphs, or even stem-archosaurs (Figure 2). Indeed, SCC traits that are statistically associated with bipedality, erect limb orientations (i.e. increase in height of the ASC), and flight (i.e. more circular ASC) are also found in the stem-archosaurs *Trilophosaurus* and *Triopticus* (Figures 1-3), which were most likely sprawling quadrupeds [54], but have poorly-understood ecologies. *Triopticus* is only known from a partial skull [41] whereas *Trilophosaurus* is hypothesized as being arboreal [54, a habit that may be linked to SCC morphology [see e.g., 24]). The small SCC sizes of these stem-archosaurs argues against the possibility that their avemetatarsalian-like SCC shapes enhanced overall vestibular sensitivity. Based on these observations, we urge strongly against the practice of interpreting specific, detailed aspects of locomotion or foraging styles of extinct taxa from SCC geometry (as done by e.g. [41,50,53]).

Evolution of the archosaur labyrinth.

Our results provide new insights into the evolution of the archosaur labyrinth. Stem-archosaurs show widely-varying labyrinth morphologies (Figure 4). Variation in relative SCC size, in both stem-archosaurs and stem-crocodylians, exceeds that seen in crocodylians (Figure S8A). This indicates an unanticipated level of variation in vestibular sensitivity, suggesting that early archosaurs had a wider range of locomotor capabilities or behaviors, consistent with suggestions of an underappreciated early morphological disparity of stem-archosaurs [40,54].

Key features of the avian SCCs have their origins among early avemetatarsalians, and may, in part, have been key to the evolutionary success of the avian stem lineage. These include large labyrinths with relative sizes that are similar to those observed among living birds and imply enhanced agility or visual acuity near the origin of Avemetatarsalia. Among crown-group archosaurs, early avemetatarsalians and pseudosuchians show little overlap of labyrinth morphology, indicating a deep evolutionary split in archosaurian SCC structure (Figure 2b). In general, labyrinth geometries of the extant archosaurs, i.e., birds and crocodylians, are not representative of the variation seen on their stem lineages.

Our findings suggest a new model for archosaurian labyrinth evolution that substantially departs from the notion that birds have highly-derived, flight-related labyrinth geometry, contrasting with a plesiomorphic crocodylian condition that remained basically unaltered since the origin of the archosaur lineage [31]. Indeed, extinct pseudosuchians show surprising variation in labyrinth geometry, contrasting with the low disparity and generalized ‘reptilian’ SCC morphology of extant crocodylians. Despite its similarity to other extant reptiles, the geometry of the crocodylian labyrinth does not result from maintenance of a plesiomorphic reptilian, or even archosaurian condition. We also reject the hypothesis that the SCC geometry of extant crocodylians results from functional optimization for aquatic life [32,51].

Beyond Archosauria, very little is known about the labyrinth of early reptiles in general (e.g. [55,56]), and the assumption that the SCC geometry of other extant groups of non-avian reptiles (i.e., lepidosaurs, turtles) represents plesiomorphic retention should also be taken with

caution. Indeed, the labyrinth geometry of the extinct early turtle *Australochelys* is more similar to that of pseudosuchians than to that of extinct and living turtles in our dataset (see Supplemental Information – Figure S2). This suggests that similarities among the labyrinths of extant non-avian reptiles, when compared to birds, might result from convergent evolution, most likely associated to spatial constraints imposed by braincase dimensions or architecture. Nevertheless, the disparate sizes of the SCCs among Triassic archosauromorphs suggest a burst of ecomorphological exploration at the early stages of the group evolutionary history (perhaps common to the deeper evolutionary history of reptiles). Finally, our findings highlight the importance of fossils to understand the patterns behind the evolution of living forms [57,58], including their sensory adaptations.

ACKNOWLEDGEMENTS

We are greatly thankful to the four anonymous reviewers for their comments, which helped to improve the overall quality of this paper. We thank Cecilia Apaldetti, Candice Stefanic, Christian Kammerer, Daniel C. Cavallari, Kenneth Bader, Matthew Brown, Matthew Colbert, Pia Viglietti, and Rodrigo T. Müller for providing relevant information. M.B. was supported by a FAPESP (São Paulo Research Foundation) Post-doctoral Fellowship (2018/18145-9) and a CNPq (National Council for Scientific and Technological Development) Junior Post-doctoral Fellowship (170867/2017-0) and also received support from the Department of Geosciences at Virginia Tech University. Parts of this work were funded by the European Union's Horizon 2020 research and innovation program 2014–2018 under grant agreement 677774 (European Research Council [ERC] Starting Grant: TEMPO) to R.B.J.B; by FAPESP under grant 2014/03825-3 to M.C.L.; by Agencia Nacional de Promoción Científica y Técnica (PICT 2018-01186 to M.D.E. and PICT 2016-0481 to A.P.-C.); by the South African National Research Foundation (grants 98800, 118794 to J.N.C.); by the Centre of Excellence, Palaeosciences (J.N.C, K.N.D, V.J.R); by the U. S. National Science Foundation (grants IOB-0517257, IOS-1050154, and IOS-145650 to L.M.W. and EAR-1337291 to S.J.N.); and by Financiadora de Estudos e Projetos—FINEP, Ministry of Science, Technology, Innovation and Communication, Brazilian Federal Government, project CT- INFRA 01/2013.

AUTHOR CONTRIBUTIONS

M.B., R.B.J.B. and S.J.N. designed the project; M.B., R.B.J.B., S.W.E., M.D.E., J.C., K.N.D., A.P.-C., V.J.R., G.S., M.R.S. and L.M.W. processed and sampled CT data; M.B., R.B.J.B., M.D.E. and S.J.N. compiled cranial measurements and details on locomotor habits of extinct taxa; S.W.E. conducted the landmarking process; R.B.J.B. conducted the analyses; M.B, R.B.J.B, S.W.E and S.J.N, wrote the bulk of the manuscript; M.B., R.B.J.B, S.W.E. and S.J.N made figures; all authors contributed to the writing, discussion and conclusion.

DECLARATION OF INTERESTS

The authors declare no competing interests.

349
350
351

FIGURE AND TABLE LEGENDS

Figure 1. Simplified phylogeny of archosauromorphs highlighting morphological diversity of the semicircular canals in selected extinct and extant species: (A) *Aquila chrysaetos,* (B) *Megapnosaurus rhodesiensis,* (C) *Plateosaurus* sp., (D) *Asilisaurus kongwe*, (E) *Ornithocheirus* sp., (F) *Allkaruen koi,* (G) *Teleocrater rhadinus,* (H) *Parasuchus hislopi,* (I) *Saurosuchus galilei,* (J) *Arizonasaurus babbitti,* (K) *Protosuchus haughtoni,* (L) *Crocodylus porosus,* (M) *Triopticus primus,* (N) *Euparkeria capensis,* (O) *Mesosuchus browni,* (P) *Trilophosaurus buettneri.*

Figure 2. Semicircular canals morphospace from principal components analyses. (A) full sample of N = 82 living and extinct reptiles and (B) reduced dataset with N = 50 species (including only archosauromorphs and fewer birds) intended to show variation primarily among extinct archosauromorphs in relation to living crocodylians and birds. Both yield similar overall patterns, but the reduced sample provides a clearer evaluation of the archosauromorph SCCs shape space. In 'A', convex hulls are associated only with extant taxa of the respective lineages. In 'B', the convex hulls associated to the extinct members of Avemetatarsalia and Pseudosuchia are displayed with lighter shades in relation to the hulls associated to the extant members of the respective lineages.

Figure 3. Landmark configurations. (A) Landmark configurations corresponding to the mean shape (grey symbols) and deformations along principal component axes PC1–PC2 (colored symbols). Deformations correspond to the highest negative ('min') and positive ('max') score on each PC axis. (B) Landmark configurations showing shape deformations for explanatory variables in the model (Table 1): shape ~ stance (non-erect | erect) + flying + postrostral length:centroid size. The shape deformation associated with postrostral length:centroid size indicates shape changes associated with relative enlargement ('large labyrinth') or reduction ('small labyrinth') of the labyrinth in relation to postrostral skull length. All labyrinths are displayed in left lateral view. PCA shape deformations are based on the full taxon set but are highly similar to those for the reduced taxon set.

Figure 4. Evolution of labyrinth size in archosauromorphs by ancestral trait estimation on a time-scaled phylogeny. Relative variation in labyrinth size is depicted based on the residuals of the best model in Table 2 (labyrinth centroid size ~ postrostral skull length). Ancestral state estimation was conducted using the ace() function of the R package ape version 5.0.

Table 1. Phylogenetic Procrustes distance regressions comparing explanations of archosauromorph labyrinth shape. Selected results discussed in the text are shown. Continuous-valued traits are log_{10}-transformed prior to analysis (postrostral length, centroid size). Significant p-values are asterisked. Results for the full set of models are included in the Supplemental Information (Table S2). N = 44 for all analyses.

Table 2. Phylogenetic regressions comparing explanations of archosauromorph labyrinth size using size-related traits. Continuous-valued traits are log_{10}-transformed prior to analysis (centroid size, postrostral length, centroid size, skull length). Significant p-values are asterisked. N = 57 for all analyses.

Table 3. Phylogenetic regressions comparing explanations of archosauromorph labyrinth size using size-related and locomotor traits after reducing consistently non-significant variables to maximise available sample size to N = 52. Continuous-valued traits are log_{10}-transformed prior to analysis (centroid size, postrostral length). Significant p-values are asterisked. Only models with non-negligible AICc weights (> one-eight of the best model) are shown. Results for the full set of models and variables are included in Appendix Table S6, and similar results for a smaller set of taxa (N = 44), in which all size and locomotor traits are known are included in Appendix Table S7.

STAR METHODS

RESOURCE AVAILABILITY

Lead Contact

Mario Bronzati (mariobronzati@usp.br).

Materials Availability

This study did not generate new unique materials.

Data and Code Availability

The 3D models of the semicircular canals of the inner ear used for the analyses, alongside details on specimens used in the study, are deposited in the public repository MorphoSource.org: [https://www.morphosource.org/projects/000349958].

The data and script required to replicate the analyses of this paper are available at the public repository OpenScienceFramework: https://osf.io/dnku4/?view_only=fe046763a7b94f4690a2fa9111dedba0.

METHOD DETAILS

Dataset

We quantified morphology of the SCCs in 37 Mesozoic archosauromorphs, nine extant crocodylians, 18 extant birds, six extant lepidosaurs, and six extinct and seven extant turtles based on micro-CT imaging and 3D geometric morphometrics. Most of our CT scan data of archosauromorphs come from previous studies, to which we added the following taxa: the stem-archosaurs *Prolacerta broomi* and *Trilophosaurus buettneri*; the pseudosuchians *Arizonasaurus babbitti, Protosuchus haughtoni,* and *Sphenosuchus acutus*; and the avemetatarsalians *Asilisaurus kongwe, Dromomeron gregorii, Heterodontosaurus tucki, Ixalerpeton polesinensis, Megapnosaurus rhodesiensis*, and *Teleocrater rhadinus*.

Our investigation focused on the early evolution of the SCC morphology in Archosauria and its sub-groups, and on how the morphology of the SCCs in early archosaurs compares to that of living reptiles. For that, data selection for extinct taxa aimed to include the earliest representatives of morphologically disparate archosaur lineages for which 3D models of the SCCs were available. Nevertheless, data for the Late Cretaceous theropod dinosaur *Velociraptor mongoliensis*, a much younger taxon and a closer relative to living birds than other taxa in our sample, was also included. The inclusion of this more bird-like, but non-flying, taxon improves our test of the association between flight origins and changes to labyrinth morphology.

Landmarks

We characterized the course of each semicircular canal using sliding semilandmarks on left labyrinths (or reflected landmarks of right labyrinths) of the studied taxa. Landmarking and computation of the midline skeleton ("autoskeleton") of each canal was done using Avizo 9. Applying this procedure is straightforward in birds and most mammals (e.g. [21,59]), in which membranous ducts are contained within individual, well-defined bony (endosseous) canals that closely match their courses. However, in many non-avian reptiles, large parts of the LSC and PSC are jointly housed in an endosseous chamber with the vestibule (e.g. 60). This results in apparent differences of endosseous structure that mask similarities in the true geometry of the membranous ducts of birds and non-avian reptiles (e.g. [36]). We therefore reconstructed the geometries of the membranous ducts of non-avian reptiles from their endosseous canal sections (Supplemental Information - Figure S1), using the approach of Evers et al. [60]. This makes use of external ridges on the labyrinth endocast combined with knowledge of conserved aspects of membranous duct morphology (e.g. [36,60]).

We placed open semilandmark curves for each semicircular canal, starting at the intersection of the canal with its ampulla, and ending at its intersection with the common crus. In total, these start and end points represent six, fixed, single-point landmarks, some of which were inferred rather than observed directly for non-avian reptiles (Supplemental Information - Figure S1). For example, the posterior ampulla was estimated to be the ventralmost point on the trajectory of the reconstructed PSC, and the intersection of the LSC with the common crus was estimated to be directly ventral to the intersection of the posterior canal with the common crus [62].

These midline skeleton landmarks were augmented by a closed loop of semilandmarks around the inner surface of the anterior canal to capture variation in relative canal thickness (e.g. [22]). Only the ASC was landmarked in this way, because the PSC and LSC intersect one another in their ventral and posterior ends in taxa in which parts of the LSC and PSC are housed together in a shared endosseous canal, meaning that the landmarks are difficult to place objectively in a comparable way among species.

Our initial landmarking involved placing arbitrary numbers of points in each semilandmark series to characterize their geometry according to complexity. We then resampled these to equal numbers of points in each specimen using the 'digit.curves' function of the R package Geomorph version 3.2.1 [61]: ASC midline skeleton (9 points), PSC midline skeleton (8 points), LSC midline skeleton (10 points), and ASC inner loop (13 points). Each midline skeleton represents the mean endolymph flow path through a semicircular canal [44] and landmarking of midline skeletons of all three canals captures their relative lengths, orientations, and morphology.

For most specimens used in this study, 3D models generated from segmentation were complete enough to be directly processed using our canal separation and reconstruction procedure. However, three models had to be reconstructed prior to this step, because parts of the labyrinth were not preserved or disarticulated. For the stem-archosaur *Chanaresuchus bonapartei*, partial right and left labyrinths were reconstructed. The right labyrinth is basically

complete, but the dorsal section of the labyrinth, including the *common crus* and dorsal sections of the anterior semicircular canals (ASC) and posterior semicircular canals (PSC), was disarticulated from the rest of the labyrinth. The common crus section was digitally re-articulated to the remaining labyrinth part in Blender 2.79b. The left labyrinth, in which the common crus part of the labyrinth was articulated but large parts of the ASC and lateral semicircular canal (LSC) were missing, was used for verification during this step. Small gaps in the reconstructed Blender model between the ventral end of the common crus and the ventral part of the labyrinth were digitally filled in Avizo Lite 9.2.0. For the dinosauriform *Lewisuchus admixtus*, the left labyrinth was generally better preserved than the right one. However, parts of the central section of the ASC were missing on the left side. The missing section was manually reconstructed in Avizo. For the dinosaur *Gnathovorax cabreirai*, the left labyrinth, which was more completely preserved than the right one, was digitally separated from the braincase endocast in Avizo. The posterior portion of the LSC was reconstructed by extending the preserved parts of the LSC to the common crus, whereas the missing section was reconstructed to be in the same horizontal plane as the visible parts of the LSC. This section was reconstructed with a low curvature, following the morphology of the closely related taxon *Herrerasaurus ischigualastensis*.

3D morphometrics

Our morphometric and statistical analyses were conducted in R version 3.6.0 (R Core Team 2019), primarily using geomorph version 3.2.1 [61] and RRPP 0.4.1 [62,63] packages. Landmarks constellations were submitted to generalized Procrustes superimposition using the gpagen function of geomorph. Semilandmarks were allowed to slide during superimposition to minimize bending energy differences from the mean shape. We used principal components analysis (PCA) of Procrustes coordinates (i.e. 3D shape data) to visualize shape variation among all specimens and also for a reduced dataset including only birds, crocodylians, and extinct archosauromorphs. Disparities (Procrustes variances) were compared using the morphol.disparity function of geomorph based on 1,000 permutations.

Comments on the determination of the types of posture, terrestrial locomotion, flight capabilities, and aquatic locomotion in extinct taxa of the dataset

Taxa in our dataset were classified in four different categories (posture, terrestrial locomotion, flight, and swimming capabilities) related to locomotor aspects (Supplemental Information - Table S1). Some 3D models of the semicircular canals are derived from specimens (e.g. *Megapnosaurus rhodesiensis* QG 195; *Ornithocheirus* sp. CAMSM SMC B54405) that preserve only the braincase or skull, with no associated postcranial material. In these cases, when possible, the classification within the four categories was based on more complete specimens of the same species/genus. Exceptions were the phytosaur *Wannia scurrienis* and the pterosaur *Allkaruen koi*, which lack more complete specimens, but their placement within the respective groups, Phytosauria and Pterosauria, safely allows their classification within the four categories used here

(see Supplemental Information - Table S1). Some taxa were scored as 'unclassified' or '?' for locomotor categories when insufficient data were available (e.g. *Triopticus primus*). These taxa were omitted from analyses that made use of that variable.

Posture

We classified the posture of taxa in our dataset (Supplemental Information - Table S1) in three widely employed postural grades [64]: sprawling, semi erect, and fully erect; respectively equivalent to sprawlers, semi-improved, and improved of Charig [6]. Previous studies have warned against the use of discrete states to standardize postural types, arguing that postural grades are better classified in a continuum, rather than as explicit discrete states (e.g. [8]). However, given the difficulties to score postural grades as a continuum in our dataset (i.e. many taxa are represented by incomplete materials and there are very few studies on their locomotor biomechanical properties), we opted to discretize postural grades in order to maximize the number of taxa for the statistical hypothesis tests. Furthermore, the three different categories used here satisfactorily reflect major differences in the locomotor style among most taxa of our sample. To avoid inconsistencies and ambiguity, we employed an explicit method in order to determine the postural grade of each taxon, based on the features detailed below. The assignment of each taxon to those grades was based on personal observations of the specimens (MB, RBJB, MDE, MCL, MRS, SJN).

- **Sprawling:** In taxa with this type of posture, the humerus and femur are mainly orthogonal to the sagittal plane (e.g. lizards, *Prolacerta*, *Proterosuchus*, rhynchosaurs). These taxa typically exhibit both the glenoid fossa (in the shoulder) and the acetabulum (in the pelvic girdle) facing laterally, a poorly differentiated femoral head, an internal trochanter in the femur, and a laterally oriented tuber in the calcaneum.

- **Semi-erect**: In taxa with this type of posture, neither the humerus and femur are mainly orthogonal to the sagittal plane, nor the plane of action of the limbs is strictly parasagittal (e.g. extant crocodylians, phytosaurs, *Euparkeria,* proterochampsids). These taxa typically exhibit a distinct but not medially offset femoral head, a fourth trochanter, and a posterolaterally to posteriorly oriented tuber in the calcaneum.

- **Erect**: In taxa with this type of posture, the humerus and femur are mainly parallel to the sagittal plane (e.g. birds, non-avian dinosaurs, aetosaurs, non-crocodylomorph loricatans). These taxa typically have either a distinctly anteromedially offset femoral head (e.g. dinosaurs) or a ventrally facing acetabulum (e.g. aetosaurs, loricatans), a fourth trochanter, and a calcaneal tuber that is either posteriorly oriented (e.g. *Asilisaurus*) or absent (e.g. most dinosaurs).

Bipedal | quadrupedal stances

This parameter is related to the two categories of terrestrial locomotion employed in our dataset (Supplemental Information - Table S1), bipedalism and quadrupedalism. It is thus independent of the parameters dealing with flight and swimming capabilities.

Flight capabilities

Among extinct taxa in our dataset, flight evolved only in pterosaurs (Supplemental Information - Table S1), and their status as active fliers is consolidated [7]. Flight also occurs in most birds.

Swimming capabilities

Among extinct taxa in our dataset, semi-aquatic lifestyle evolved in phytosaurs [65] and in thalattosuchian crocodyliforms [66]. These taxa typically exhibit a set of features also observed in modern crocodylians, such as the presence of an elongated rostrum, a flattened skull, external nares facing dorsally, and rugose skull surface; and are also commonly found in fluvial to shallow marine deposits [65,66]. Two taxa in our analysis exhibit skulls with some of the features described above, *Proterosuchus fergusi* and *Chanaresuchus bonapartei*, but their status as semi-aquatic animals are still inconclusive [67-69].

Labyrinth size

Labyrinth centroid size was compared against two cranial measurements, skull length and postrostral length (Table S1). Skull length corresponds to the length from the anterior tip of the snout to the posterior tip of the occipital condyle. Postrostral length corresponds to the length from the anterior margin of the orbit to the posterior tip of the occipital condyle. Some specimens in our dataset lack either a complete skull or the postrostral portion of it. When possible, estimates (length based on estimates are highlighted with * in Table S1) for skull and postrostral lengths of these incomplete specimens were based on comparisons of the dimension of their preserved skull bones with the same bones of specimens of the same species or genus having a complete (or more complete) skull. When that was not possible, skull size was inferred based on relative dimensions of other closely related taxa known from more complete specimens.

QUANTIFICATION AND STATISTICAL ANALYSIS

Statistical hypothesis tests

We evaluated the relationships of archosauromorph labyrinth size and geometry with various explanatory variables using regression-based phylogenetic comparative methods [70-72]. These tests were conducted using only information for archosauromorphs from our dataset; it

therefore does not include turtles and lepidosaurs, which were included in our PCA for comparative purposes. We used a composite phylogeny with branch lengths as the phylogenetic framework for these analyses using functions in the R packages phytools version 0.7-47 [73] and paleotree version 3.3.25 [74], combining previous trees for early archosauromorphs [75], crocodylomorphs [76], dinosaurs [77], pterosaurs [78], and a phylogenomic bird tree [79]. Modifications to stratigraphic age data and topology of our sampled taxa were made based on recent studies of early archosauromorphs (e.g. [4,75,80]). Polytomies were resolved at random resulting in a distribution of 25 trees. Divergences among extinct taxa were calibrated to time using the minimum branch length criterion ('mbl'; e.g. [81]), setting zero-length branches to a minimum length of 1 Ma. Because of the sparse taxon sample for which we have data, the divergence times between pairs of sampled taxa are generally determined by the stratigraphic ages of older extinct taxa, and not by the mbl criterion.

Our explanatory variables included: (1) Size variables intended to capture the effects of allometry and the potential influence of spatial constraint in the braincase on labyrinth morphology, including basal cranial length, postrostral cranial length, and labyrinth centroid size, which were $\log_{10}$-transformed prior to analysis. (2) Locomotion-related categorical variables such as flight | non-flight, primitive sprawling | semi-erect | erect limb postures, bipedal | quadrupedal gait, and semi-aquatic | terrestrial habits. These were scored using published inferences from the literature and also personal observation of the materials (see Supplemental Information – Table S1), allowing missing data scores (inapplicable: 'NA') when insufficient data were available (e.g., when postcranial bones were not preserved). (3) A skull geometry variable, the dorsoventral height to mediolateral width aspect ratio of the posterior part of the skull, to test links between labyrinth geometry and posterior skull geometry. Sample sizes were dependent on data availability for locomotor and skull size or geometry traits (see Supplemental Information – Data S1A-C). We evaluated the many combinations of these variables as explanations of both size and shape variation among archosauromorph labyrinths.

Statistical explanations for labyrinth centroid size were tested using phylogenetic generalized least squares regression (pGLS), estimating lambda, the phylogenetic signal parameter [82], during the estimation of regression parameters. Models were compared using Akaike's information criterion for finite sample size and Akaike weights (AICc weights [83]). Because of missing data in some locomotion variables (see above), our initial analyses using all variables included only those taxa for which all variables could be scored (N = 44 archosauromorph taxa). This set of analyses identified skull length, postrostral skull length, semi-erect | erect limb postures and bipedal | quadrupedal stance as potential correlates of labyrinth centroid size (Supplemental Information - Data S1F). This subset of traits was carried forward to a second round of analysis using the larger set of N = 52 taxa, the results of which are reported in the main text (Supplemental Information - Data S1E). Analyses of the allometry of labyrinth centroid size were also conducted on the full set of N = 57 taxa for which labyrinth centroid size and measures of skull length were known (Table 2). The residuals from this latter analysis were used to document the evolution of relative labyrinth size among early archosaurs

using maximum-likelihood ancestral character estimation methods [80,84] via the ace() function of the package ape version 5.0 [85].

Statistical explanations for labyrinth shape were tested using Procrustes-distance-based phylogenetic regressions [72], implemented in the procD.pgls function of geomorph [63] using the type II sum of squares. Our analyses included the N = 44 taxa for which all size and locomotion traits were scored. AICc is not available for procD.pgls so we compared models informally based on their R^2 values and the p-values of their component variables through an iterative process of model construction. We initially investigated relations of size traits (skull length, postrostral skull length, labyrinth centroid size) as correlates of labyrinth shape, exploring the effects of allometry (e.g. shape ~ size), independent effects of size traits (e.g. shape ~ skull length + labyrinth centroid size) and the potential for non-independent effects signified by interaction terms as embodied by the following model equation: shape ~ skull length:labyrinth centroid size; which represents the hypothesis that taxa with proportionally larger labyrinths in relation to skull size have different shaped labyrinths. This could occur either due to constraints on labyrinth shape imposed by space restrictions or due an influence of selection for increased vestibular sensitivity having inter-linked effects on both labyrinth shape and size. These analyses determined the absence of straightforward allometric effects. Nevertheless, we also found evidence for a significant effect of an interaction term between postrostral skull length and labyrinth centroid size (Supplemental Information - Data S1F), suggesting that labyrinth size relative to skull size has an effect on labyrinth shape. This interaction term was carried forward to our analysis of locomotor traits.

Effect of locomotion traits on labyrinth shape was evaluated individually and in all combinations using models of two forms: (1) shape ~ locomotion traits; (2) shape ~ postrostral skull length:labyrinth centroid size + locomotion traits. The second expression simultaneously accounts for locomotion-related variation in labyrinth shape, and variation in labyrinth shape with the proportional labyrinth size, and was universally better-supported by R^2 and statistical significance (p-values). The full set of results across all the models we tested is given in Data S1A (Supplemental Information).

Functional interpretation of shape deformations

We visualized the idealized shape deformation associated with specific locomotor traits (flight, bipedality, erect limb orientations) by modifying the mean labyrinth shape using the coefficients for locomotor traits as returned by the following procD.pgls models: (1) shape ~ bipedal + flying + postrostral length:centroid size and (2) labyrinth shape ~ stance + flying + postrostral length:centroid size. Functional interpretations were based on quantifying the canal lengths and inter-SCC plane angles using custom scripts in R. Canal lengths were calculated as the summed point-to-point distances for the ASC, PSC and LSC between the ampulla and common crus (ASC and PSC) or ampulla and vestibule (LSC).

DATA S1 Legend.

Spreadsheets containing the full results of the statistical analyses conducted in this study.

REFERENCES

01. Nesbitt, S.J. (2011). The early evolution of archosaurs: relationships and the origin of major clades. Bull. Am. Mus. Nat Hist. *352*, 1-292.
02. Huey, R.B. (1982). Temperature, physiology, and the ecology of reptiles. In Biology of the Reptilia, C. Gans, F.H. Pough, eds. (Cambridge, USA: Academic Press), pp. 25-91.
03. Liem, K.F., Bemis, W.E., Walker, W.F., and Grande L. (2001). *Functional Anatomy of the Vertebrates* (Boston, USA: Thomson Learning).
04. Ezcurra, M.D., and Butler R.J. (2018). The rise of the ruling reptiles and ecosystem recovery from the Permo-Triassic mass extinction. Proc. R. Soc. B. *285*, 20180361 (2018).
05. Gauthier, J.A., Nesbitt, S.J., Schachner, E.R., Bever, G.S., and Joyce, W.G. (2011). The bipedal stem crocodilian *Poposaurus gracilis*: inferring function in fossils and innovation in archosaur locomotion, Bull. Peabody. Mus. Nat. Hist. *52(1)*, 107-126.
06. Charig, A.J. (1972). The evolution of the archosaur pelvis and hind-limb: an explanation in functional terms. In Studies in vertebrate evolution: Essays presented to Dr. F. R. Parrington, FRS, K.A. Joysey, and T.S. Kemp, eds. (Edinburgh, UK: Oliver & Boyd), pp. 121–155.
07. Padian, K. (1985). The origins and aerodynamics of flight in extinct vertebrates. Palaeontology. *28*, 413–433.
08. Gatesy, S.M. (1991). Hindlimb movements of the American alligator (*Alligator mississippiensis*) and postural grades. J. Zool. *224*, 577–588.
09. Bates, K.T., and Schachner, E.R. (2012). Disparity and convergence in bipedal archosaur locomotion. J. R. Soc. Interface. 9(71), 1339–1353.
10. Bonaparte, J.F. (1984). Locomotion in rauisuchid thecodonts. J. Vertebr. Paleontol. *3*, 210–218.
11. Hutchinson, J.R. (2006). The evolution of locomotion in archosaurs. Comptes Rendus Palevol. *5*, 519–530.
12. Kubo, T., and Kubo, M.O. (2012). Associated evolution of bipedality and cursoriality among Triassic archosaurs: a phylogenetically controlled evaluation. Paleobiology, *38(3),* 474-485.
13. Müller, J., Bickelmann, C., and Sobral, G. (2018). The evolution and fossil history of sensory perception in amniote vertebrates. *Annu. Rev. Earth Planet. Sci. 46*, 495-519.
14. Bilo, D., and Bilo, A. (1978). Wind stimuli control and vestibular and optokinetic reflexes in the pigeon. Naturwissenschaften. *65*, 161–162.
15. Wilson, V.J., and Melville-Jones, G. (1979). Mammalian Vestibular Physiology. (Berlin, Germany: Springer).
16. Leigh, J., and Brandt, T. (1993). A re-evaluation of the vestibule-ocular reflex: new ideas of its purpose, properties, neural substrate and disorders. Neurology, *43*, 1288–1295.
17. Spoor, F. (2003). The semicircular canal system and locomotor behaviour, with special reference to hominin evolution. Cour. Forsch. Senckenberg. *243*, 93–104.
18. Witmer, L.M., Chaterjee, S., Franzosa, J., and Rowe, T. (2003). Neuroanatomy of the flying reptiles and implications for flight, posture and behaviour. Nature. *425*, 950-953.
19. Walsh, S.A., and Milner, A.C. (2011). Evolution of the avian brain and senses. In Living Dinosaurs: the Evolutionary History of Modern Birds, G. Dyke, and G. Kaiser, eds. (New Jersey, US: John Wiley) pp. 282–305.
20. Georgi, J., Sipla, J.S., and Forster, C.A. (2013). Turning semicircular canal function on its head: dinosaurs and a novel vestibular analysis. PLoS ONE, *8*, e58517.
21. Benson R.B.J., Starmer-Jones, E., Close, R.A., and Walsh, S.A. (2017). Comparative analysis of vestibular ecomorphology of birds. J. Anat. *231*, 990-1018.
22. Neenan, J.M., Reich, T., Evers, S.W., Druckenmiller, P.S., Voeten, D.F.A.E., Choiniere, J.N., Barrett, P.M., Pierce, S.E., and Benson, R.B.J. (2017). Evolution of the sauropterygian labyrinth with increasingly pelagic lifestyles. Curr. Biol. *27*, 3852-3858.
23. Spoor, F., and Zonneveld, F. (1998). Comparative review of the human bony labyrinth. *Am.* J. Phys. Anthropol. *41*, 211–251.

24. Spoor, F., Garland, T., Krovitz, G., Ryan, T.M., Silcox, M.T., and Walker, A. (2007). The primate semicircular canal system and locomotion. Proc. Natl. Acad. Sci. U.S.A. *104*, 808–812.
25. Spoor, F., Bajpai, S., Hussain S.T., Kumar, K., and Thewissen, J.G.M. (2002). Vestibular evidence for the evolution of aquatic behaviour in early cetaceans. Nature, *417*, 163–166.
26. Malinzak, M.D., Kaya, R.F., and Hullar, T.E. (2012). Locomotor head movements and semicircular canal morphology in primates. Proc. Natl. Acad. Sci. U.S.A. *109*, 914–919.
27. Kemp, A.D., and Kirk, E.C. (2014). Eye size and visual acuity influence vestibular anatomy in mammals. Anat. Rec*. 297*, 781–790.
28. Ekdale, E.G. (2916). Form and function of the mammalian inner ear. J. Anat. *228*, 324–337.
29. Silcox, M.T., Bloch, J.I., Boyer, D.M., Godinot, M., Ryan, T.M., Spoor, F., and Walker, A. (2009). Semicircular canal system in early primates. J. Hum. Evol. *56*, 315–327.
30. Cox, P.G., and Jeffery, N. (2010). Semicircular canals and agility: the influence of size and shape measures. J. Anat. *216*, 37–47.
31. Jones, G.M., and Spells, K.E. (1963). A theoretical and comparative study of the functional dependence of the semicircular canal upon its physical dimensions. Proc. R. Soc. Lond. B. *157*, 403–419.
32. Georgi, J.A., and Sipla, J.S. (2008). Comparative and functional anatomy of balance in aquatic reptiles and birds. In Sensory evolution on the threshold, adaptations in secondarily aquatic vertebrates, J. H. M. Thewissen, and S. Nummela, eds. (Berkeley, US: University of California Press), pp. 133-256.
33. Goyens, J. (2019). High ellipticity reduces semicircular canal sensitivity in squamates compared to mammals. Sci. Rep*. 9*, 16428.
34. Sipla J. (2007). The Semicircular Canals of Birds and Non-Avian Theropod Dinosaurs. *PhD Dissertation, Stony Brook University*.
35. Marugán-Lobón, J., Chiappe, L.M., and Farke, A.A. (2013). The variability of inner ear orientation in saurischian dinosaurs: testing the use of semicircular canals as a reference system for comparative anatomy. PeerJ *1*, e124.
36. Wever, E.G. (1978). The Reptile Ear (Priceton, US: Princeton University Press).
37. Ezcurra, M.D., Jones, A.S., Gentil, A.R., and Butler, R.J. (2021). Early Archosauromorphs: The Crocodile and Dinosaur Precursors. In Encyclopedia of Geology, 2nd edition, vol [4], D. Alderton, and S.A. Elias, eds. (United Kingdom: Academic Press).
38. Cabreira, S.F., Kellner, A.W.A., Dias-da-Silva, S., Silva, L.R., Bronzati, M., Marsola, J.C.A., Müller, R.T., Bittencour, J.S., Batista, B.J., and Raugust, T. et al. (2016). A unique Late Triassic dinosauromorph assemblage reveals dinosaur ancestral anatomy and diet. Curr. Biol. *26(22)*, 3090–3095.
39. Codorniú, L., Paulina-Carabajal, A., Pol, D., Unwin, D., and Rauhut, O.W.M. (2016). A Jurassic pterosaur from Patagonia and the origin of the pterodactyloid neurocranium. PeerJ, *4*, e2311.
40. Stocker, M.R., Nesbitt, S.J., Criswell, K.E., Parker, W.G., Witmer, L.M., Rowe, T.B., Ridgely, R., and Brown, M.A. (2016). A dome-headed stem archosaur exemplifies convergence among dinosaurs and their distant relatives. Curr. Biol*. 26*, 2674-2680.
41. Bronzati, M., Rauhut, O.W.M., Bittencourt, J.S., and Langer, M.C. (2017). Endocast of the Late Triassic (Carnian) dinosaur *Saturnalia tupiniquim*: implications for the evolution of brain tissue in Sauropodomorpha. Sci. Rep*. 7*, 11931.
42. Ezcurra, M.D., Nesbitt, S.J., Fiorelli, L.E., and Desojo, J.B. (2020). New specimen sheds light on the anatomy and taxonomy of the early Late Triassic dinosauriforms from the Chañares Formation, NW Argentina. Anat. Rec*. 303(5),* 1393-1498.
43. Rabbitt, R.D., Damiano, E.R., and Grant, J.W. (2004). Biomechanics of the semicircular canals and otolith organs. In The Vestibular System, S.M. Highstein, A. Popper, and R. Fay eds.(New Yor, USA, Springer), pp- 153-201.
44. David, R., Droulez, J., Allain, R., Berthoz, A., Janvier, P., and Bennequin, D. (2010). Motion from the past, A new method to infer vestibular capacities of extinct species. C. R. Palevol. *9*, 397–410.
45. Xu, X., Zheng, X., Sullivan, C., Wang, W., Xing, L., Wang, Y., Zhang, X., O'Connor, J.K., Zhang, F., and Pan, Y. (2015). A bizarre Jurassic maniraptoran theropod with preserved evidence of membranous wings. Nature*. 521*, 70-73.
46. Walsh, S.A., Iwanjuk, A.N., Knoll, M.A, Bourdon, E., Barrett, P.M., Milner, A.C., Nudds, R.L., Abel, R.L., and Sterpaio, P.D. (2013). Avian Cerebellar Floccular Fossa Size Is Not a Proxy for Flying Ability in Birds. PLoS ONE*, 8(6),* e67176.

47. Hadziselimnovic, H. and. Savkovic, L. (1964). Appearance of semicircular canals in birds in relation to mode of life. Acta Anat. *57*, 306–315.
48. Davies, K.T.J., Bates, P.J.J., Maryanto, I., Cotton, J.A., and Rossiter, S.J. (2013). The evolution of bat vestibular systems in the face of potential antagonistic selection pressures for flight and echolocation. PLoS ONE. *8(4),* e61998.
49. Charig, A.J. (1984). Competition between therapsids and archosaurs during the Triassic Period: a review and synthesis of current theories. Symp. Zool. Soc. Lond. *52*, 597–628.
50. Dudgeon, T.W., Maddin, H.C., Evans, D.C., and Mallon, J.C. (2020). The internal cranial anatomy of *Champsosaurus* (Choristodera: Champsosauridae): Implications for neurosensory function. Sci. Rep. *10*, 7122.
51. Schwab, J.A., Young, M.T., Neenan, J.M., Walsh, S:A., Witmer, L.M., Herrera, Y., Allain, R., Brochu, C., Choiniere, J.N. Clark, J.M., et al. (2020). Inner ear sensory system changes as extinct crocodylomorphs transitioned from land to water, Proc. Nat. Acad. Sci*., 117(19),* 10422-10428.
52. Spielmann, J.A., Heckert, A.B., and Lucas, S.G. (2005). The Late Triassic archosauromorph *Trilophosaurus* as an arboreal climber. Riv. Ital. Paleontol*. S. 111*, 395-412.
53. Schade, M., Rauhut, O.W.M., and Evers, S.W. (2020). Neuroanatomy of the spinosaurid *Irritator challengeri* (Dinosauria: Theropoda) indicates potential adaptations for piscivory, Sci. Rep*. 10*, 9259.
54. Foth, C., Ezcurra, M.D., Sookias, R.B., Brusatte, S.L., Butler, R.J. (2016). Unappreciated diversification of stem archosaurs during the Middle Triassic predated the dominance of dinosaurs. BMC Evol. Biol*. 16*, 188.
55. Gardner, N.M., Holliday, C.M., and O'Keefe, F.R. (2013). The braincase of *Youngina capensis* (Reptilia, Diapsida): new insights from high-resolution CT Scanning of the holotype. Palaeontol. Electron*. 13(3),* 19A.
56. Sobral, G., Sues, H.-D., and Müller, J. (2015). Anatomy of the enigmatic reptile *Elachistosuchus huenei* Janensch, 1949 (Reptilia: Diapsida) from the Upper Triassic of Germany and its relevance for the origin of Sauria. PLoS ONE *10(9),* e0135114.
57. Gauthier, J., Kluge, A.G., and Rowe, T. (1988). Amniote phylogeny and the importance of fossils. Cladistics *4(2),* 105-209.
58. Donoghue, M.J., Doyle, J.A., Gauthier, J., Kluge, A.G., Rowe, T. (1989). The importance of fossils in phylogeny reconstruction. Annu. Rev. Ecol. Syst*. 20*, 431-460.
59. Gunz, P., Ramsier, M., Kuhrig, M., Hublin, J.-J., and Spoor, F. (2012). The mammalian bony labyrinth reconsidered, introducing a comprehensive geometric morphometric approach. J. Anat*. 220*, 529–543.
60. Evers S.W., Neenan, J.M., Ferreira, G.S., Werneburg, I., Barrett, P.M., and Benson, R.B.J. (2019). Neurovascular anatomy of the protostegid turtle *Rhinochelys pulchriceps* and comparisons of membranous and endosseous labyrinth shape in an extant turtle. Zool. J. Linn. Soc*. 187(3),* 800-828.
61. Adams, D., Collyer, M., and Kaliontzopoulou, A. Geomorph: Software for geometric morphometric analyses. R package version 3.2.1. https://cran.r-project.org/package=geomorph. Acessed 1 May 2020.
62. Collyer, M.L., and Adams, D.C. (2018). RRPP: An r package for fitting linear models to high-dimensional data using residual randomization. Methods. Ecol. Evol*. 9(7),* 1772-1779.
63. Collyer, M.L., and Adams, D.C. RRPP: Linear Model Evaluation with Randomized Residuals in a Permutation Procedure, R package version 0.5.2. https://cran.r-project.org/package=RRPP. Accessed 1 May 2020.
64. Bakker, R.T. (1971). Dinosaur physiology and the origin of mammals. Evolution *25*, 636-658.
65. Stocker, M.R-, and Butler, R.J. (2013). Phytosauria. Geol. Soc. Spec. Publ. *379*, 91-117.
66. Wilberg, E.W., Turner, A.H., and Brochu, C.A. (2019). Evolutionary structure and timing of major habitat shifts in Crocodylomorpha. Sci. Rep. *9*, 514.
67. Ezcurra, M.D., Butler, R.J., and Gower, D.J. (2013). 'Proterosuchia': the origin and early evolution of Archosauriformes. Geol. Soc. Spec. Publ. *379*, 9-33.
68. Trotteyn, M.J., and Ezcurra, M.D. (2014). Osteology of *Pseudochampsa ischigualastensis* gen. et comb. nov. (Archosauriformes: Proterochampsidae) from the Early Late Triassic Ischigualasto Formation of Northwestern Argentina. PLoS ONE *9(11),* e111388.
69. Brown, E.E., Butler, R.J., Ezcurra, M.D., Bhullar, B.-A.S., and Lautenschlager, S. (2020). Endocranial anatomy and life habits of the Early Triassic archosauriform *Proterosuchus fergusi*. Palaeontology *63(2),* 255-282.

70. Felsenstein, J. (1985). Phylogenies and the comparative method. Am. Nat. *125, 1–15.*
71. Grafen, A. (1989). The phylogenetic regression. Philos. Trans. R. Soc. Lond. B Biol. Sci. *326(1233),* 119-57.
72. Adams, D.C. (2014). A method for assessing phylogenetic least squares models for shape and other high-dimensional multivariate data. Evolution *68*, 2675-2688-
73. Revell, L.J. (2012). phytools: an R package for phylogenetic comparative biology (and other things). Methods Ecol. Evol. *3(2),* 217-223.
74. Bapst, D.W. (2012). paleotree: an R package for paleontological and phylogenetic analyses of evolution. Methods Ecol. Evol. *3(5),* 803-807.
75. Ezcurra, M.D., Nesbitt, S.J., Bronzati, M., Dalla-Vechia, F., Agnolin, F.L., Benson, R.B.J., Brissón Egli, F., Cabreira, S.F., Evers, S.W., Gentil, A.R, et al. (2020). Enigmatic dinosaur precursors bridge the gap to the origin of Pterosauria. Nature, *588,* 445-449.
76. Godoy, P.L., Benson, R.B.J., Bronzati, M., and Butler, R.J. (2019). The multi-peak adaptive landscape of crocodylomorph body size evolution. BMC Evol. Biol., *19*, 167.
77. Benson, R.B.J., Campione, N.E., Carrano, M.T., Mannion, P.D., Sullivan, C., Upchurch, P., and Evans, D.C. (2014). Rates of dinosaur Body Mass Evolution Indicate 170 Million Years of Sustained Ecological Innovation on the Avian Stem Lineage. PLOS Biol.*12(5),* e1001853.
78. Benson, R.B.J., Frigot, R.A., Goswami, A., Andres, B., Butler, R.J. (2014). Competition and constraint drove Cope's rule in the evolution of giant flying reptiles. Nat. Comm. *5*, 3567.
79. Prum, R.O., Berz, J.S., Dornburg, A., Field, D.J., and Townsend, J.P. (2015). A comprehensive phylogeny of birds (Aves) using targeted next-generation DNA sequencing, Nature *526*, 569-573.
80. Nesbitt, S.J., Butler, R.J., Ezcurra, M.D., Barrett, P.M., Stocker, M.R., Angielczyk, K.D., Smith, R.M.H., Sidor, C.A., Niedźwiedzki, G., Sennikov, A.G., and Charig, A.J. (2017).The earliest bird-line archosaurs and the assembly of the dinosaur body plan. Nature *544*, 484–487.
81. Bapst, D.W. Assessing the effect of time-scaling methods on phylogeny-based analyses in the fossil record. Paleobiology *40*, 331-351.
82. Pagel, M. (1999). Inferring the historical patterns of biological evolution. Nature *401*, 877–884.
83. Burnham, K.P., and Anderson, D. (2002). Model Selection and Multi-Model Inference: a practical Information-Theoretic Approach. New York, US: Springer).
84. Schluter, D., Price, T., Mooers, A.Ø., and Ludwig, D. (1997). Likelihood of Ancestor States in Adaptive Radiation, *Evolution 51(6),* 1699-1711.
85. Paradis, E., and Schliep, K. (2019). ape 5.0: an environment for modern phylogenetics and evolutionary analyses in R. Bioinformatics *35*, 526-528.

KEY RESOURCES TABLE

REAGENT or RESOURCE	SOURCE	IDENTIFIER
Deposited data		
3D models of the semicircular canals and details of the specimens used in this study	https://www.morphosource.org/projects/000349958	NA
Dataset of posture, terrestrial locomotion, flight capabilities, and aquatic locomotion, labyrinth centroid size, and, selected cranial measurements	This study	TABLE S1
Data and script required to replicate the analyses	https://osf.io/dnku4/?view_only=fe046763a7b94f4690a2fa9111dedba0.	NA
Software and algorithms		
R package Geomorph V 3.2.1	https://cran.r-project.org/package=geomorph R package Geomorph V 3.2.1	NA
R package RRPP V 0.5.2.	https://cran.r-project.org/package=RRPP R package V 0.5.2.	NA
R package phytools V 0.7-47	https://cran.r-project.org/web/packages/phytools R package phytools V 0.7-47	NA
R package paleotree V 3.3.25	https://cran.r-project.org/web/packages/paleotree R package paleotree V 3.3.25	NA
R package ape V 5.0	https://cran.r-project.org/web/packages/ape R package ape V 5.0	NA
Blender V 2.79b	https://www.blender.org/	NA
Avizo Lite 9.2.0	Thermo Fisher Scientific	NA

Figure 4

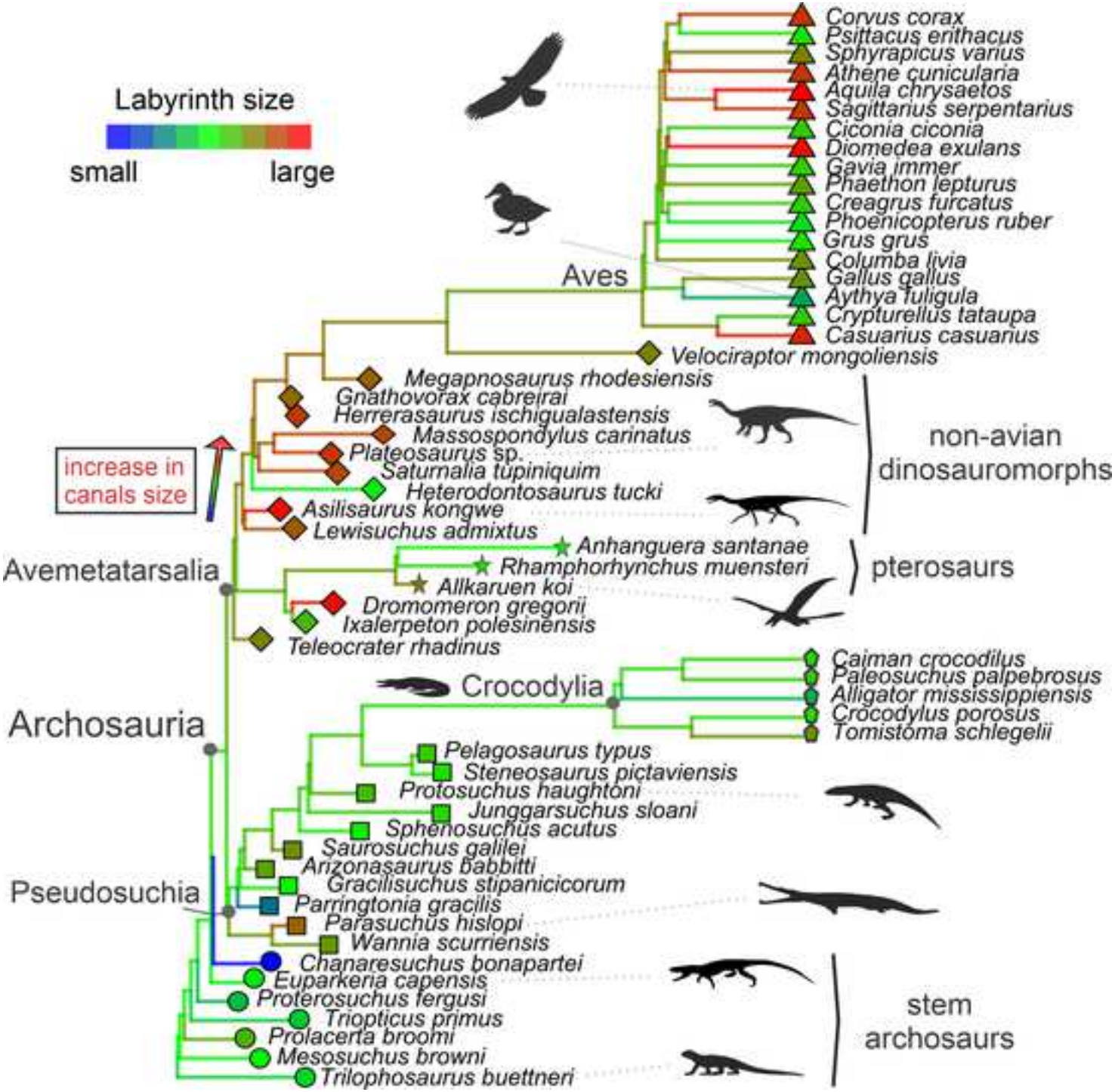

Figure 1

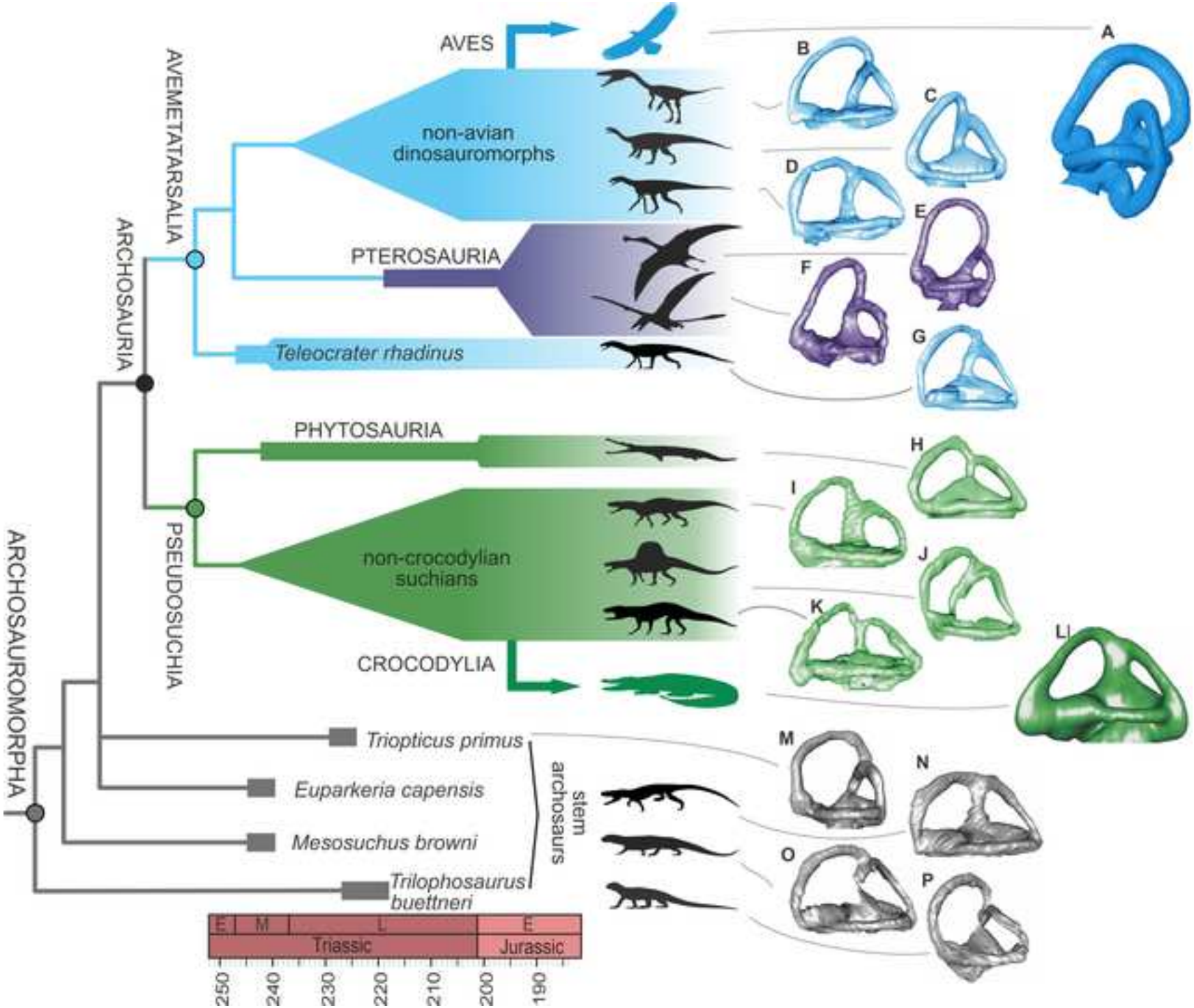

Figure 2

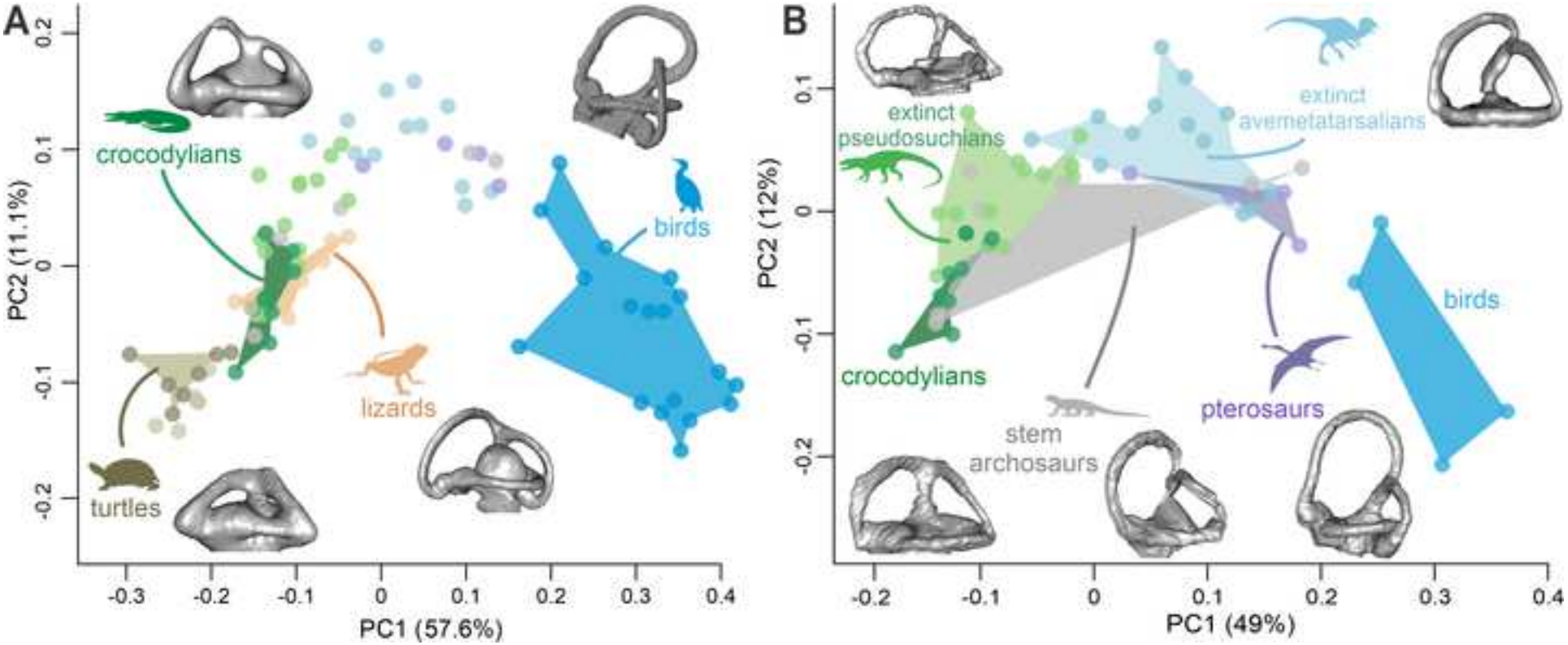

Figure 3

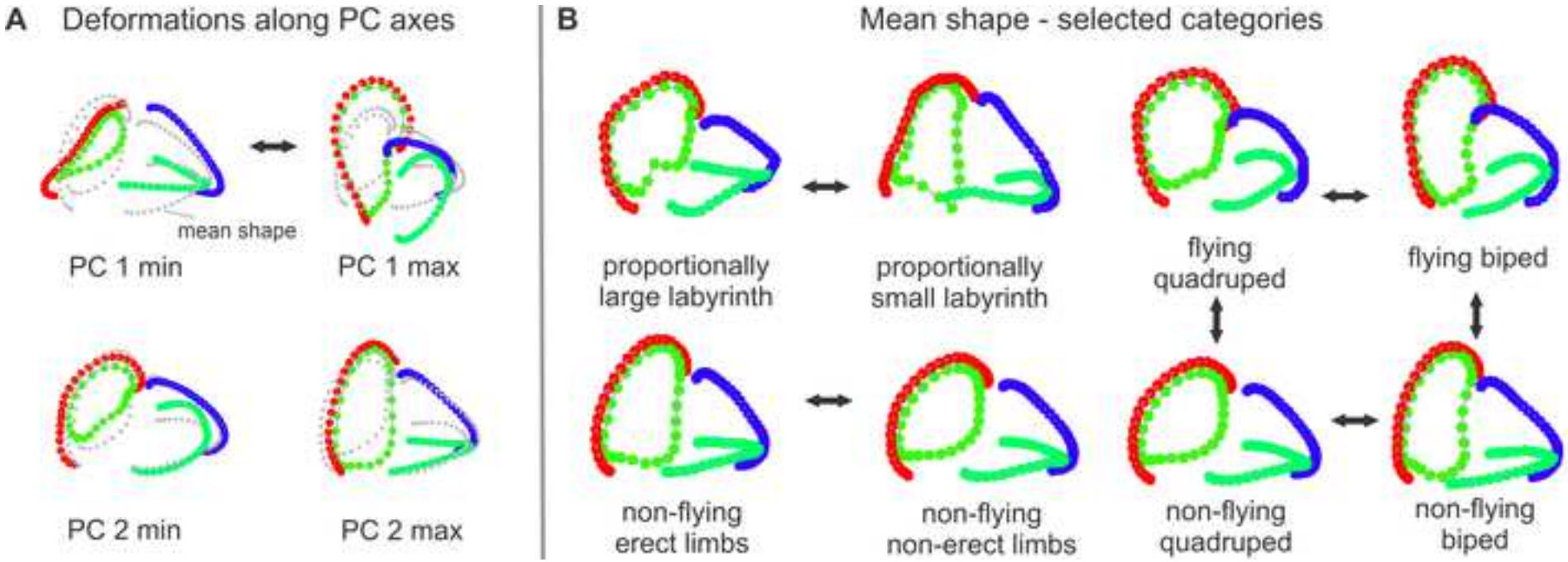

TABLES

Table 1. Phylogenetic Procrustes distance regressions comparing explanations of archosauromorph labyrinth shape. Selected results discussed in the text are shown. Continuous-valued traits are log_{10}-transformed prior to analysis (postrostral length, centroid size). Significant p-values are asterisked. Results for the full set of models are included in the Supplemental Information (Table S2). N = 44 for all analyses.

Model	Variable	Rsq	Pr(>F)
labyrinth shape ~ flying	flying	0.055	0.013*
labyrinth shape ~ stance (non-erect | erect)	stance	0.053	0.014*
labyrinth shape ~ bipedal	bipedal	0.064	0.002*
labyrinth shape ~ stance2 (sprawling | semi-erect or erect)	stance2	0.016	0.675
labyrinth shape ~ aquatic	aquatic	0.031	0.183
labyrinth shape ~ bipedal + flying + postrostral length:centroid size	postrostral length	0.042	0.018*
	centroid size	0.041	0.023*
	bipedal	0.056	0.002*
	flying	0.051	0.008*
	postrostral length: centroid size	0.046	0.015*
labyrinth shape ~ stance + flying + postrostral length:centroid size	postrostral length	0.041	0.016*
	centroid size	0.040	0.027*
	stance	0.050	0.003*
	flying	0.052	0.010*
	postrostral length: centroid size	0.063	0.001*

Table 2. Phylogenetic regressions comparing explanations of archosauromorph labyrinth size using size-related traits. Continuous-valued traits are log_{10}-transformed prior to analysis (centroid size, postrostral length, centroid size, skull length). Significant p-values are asterisked. N = 57 for all analyses.

Model	AICc	AICc weight	R^2	Lambda	Variable	Coefficient	Std. Error	t value	p value
centroid size ~ postrostral length	-97.463	0.88	0.747	0.994	intercept	0.535	0.087	6.15	<0.0001*
					postrostral length	0.588	0.043	13.704	<0.0001*
centroid size ~ postrostral length + skull length	-93.269	0.11	0.738	1.008	intercept	0.528	0.088	6.033	<0.0001*
					postrostral length	0.484	0.122	3.958	0.0002
					skull length	0.094	0.102	0.924	0.3594
centroid size ~ skull length	-87.996	0.01	0.702	1.052	intercept	0.577	0.04	14.325	<0.0001*
					skull length	0.494	0.003	173.416	<0.0001*

Table 3. Phylogenetic regressions comparing explanations of archosauromorph labyrinth size using size-related and locomotor traits after reducing consistently non-significant variables to maximise available sample size to N = 52. Continuous-valued traits are log_{10}-transformed prior to analysis (centroid size, postrostral length). Significant p-values are asterisked. Only models with non-negligible AICc weights (> one-eight of the best model) are shown. Results for the full set of models and variables are included in Appendix Table S6, and similar results for a smaller set of taxa (N = 44), in which all size and locomotor traits are known are included in Appendix Table S7.

Model	AICc	AICc weight	R2	lambda	Variable	Coef.	Std.Error	t-value	p value
centroid size ~ postrostral length	-88.682	0.65	0.755	0.982	intercept	0.575	0.086	6.703	<0.0001*
					postrostral length	0.57	0.042	13.414	<0.0001*
centroid.size ~ stance (erect|non-erect) + postrostral length	-86.415	0.21	0.755	0.894	intercept	0.663	0.086	7.75	<0.0001*
					stance	-0.075	0.03	-2.521	0.0150*
					postrostral length	0.56	0.04	13.859	<0.0001*

FIGURE S1

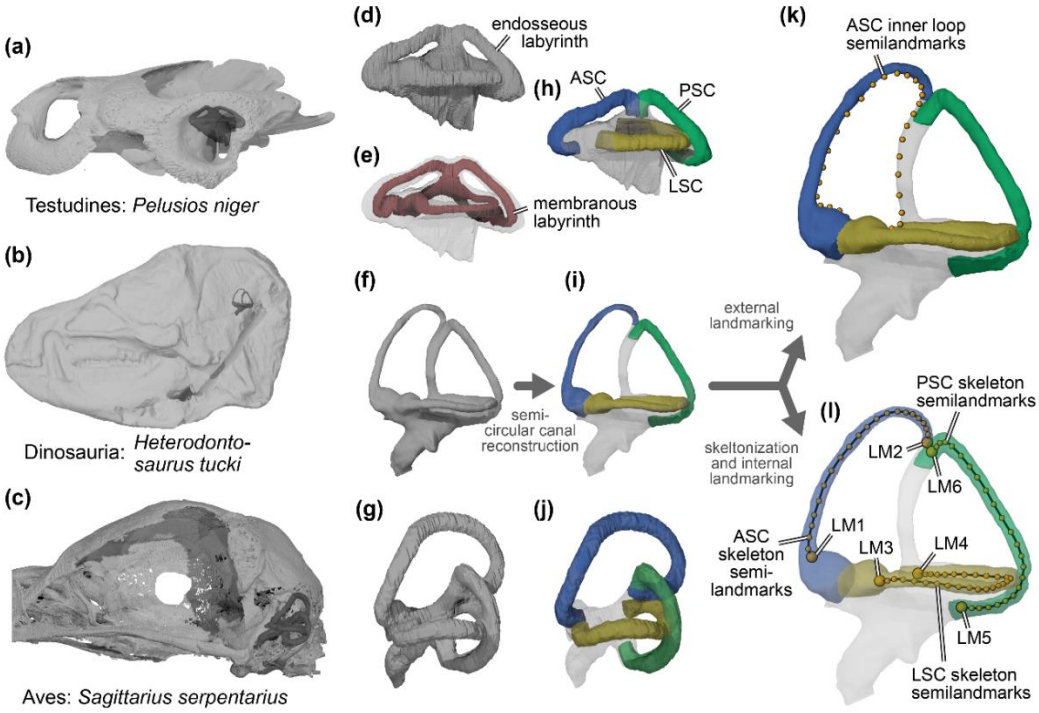

Figure S1. Labyrinth model preparation and landmarking workflow, Related to STAR Methods. (a)–(c) selected skulls ('b' reflected for comparison) with position and size of endosseous labyrinth models superimposed; (d), (f), (g) unmodified endosseous labyrinth models segmented from CT-data; (e) transparent endosseous and red membranous labyrinth model of 'd' used for verification of canal reconstructions; (h)–(j) endosseous labyrinths with colored isolated semicircular canal reconstructions, (k) illustration of external landmarks; (l) illustration of landmarks placed internally on midline 'autoskeletons' of semicircular canal reconstructions. Black lines in 'l' are midline 'autoskeletons'. Abbreviations: ASC, anterior semicircular canal; LM, landmark; LSC, lateral semicircular canal; PSC, posterior semicircular canal. Note that the skull used as model for (a) is not from *Pelusios niger*, as the dataset from which the *Pelusios ear* model was segmented did not permit the extraction of a full skull for model.

Figure S2

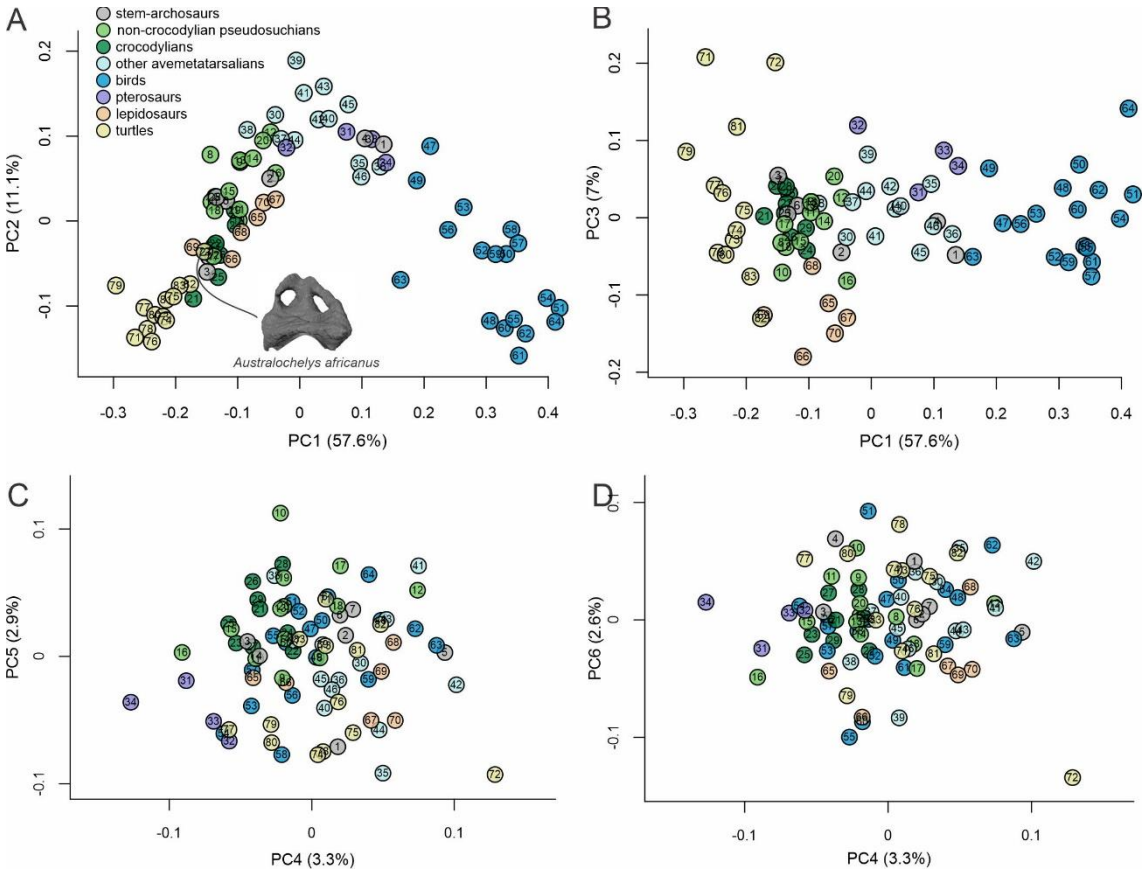

Figure S2. Plots of principal component scores from PCA of full dataset (see main text Figure 2) using numbers to indicate taxa, Related to Figure 2: (A) - PC1 vs. PC2; (B) - PC1 vs PC3, (C) - PC4 vs PC5; (D) - PC4 vs PC6. **Stem-archosaurs:** 1 - *Trilophosaurus buettneri*, 2 - *Mesosuchus browni*, 3 - *Prolacerta broomi*, 4 - *Triopticus primus*, 5 - *Proterosuchus fergusi*, 6 - *Euparkeria capensis*, 7 - *Chanaresuchus bonapartei*, **Non-crocodylian pseudosuchians**: 8 - *Wannia scurriensis*, 9 - *Parasuchus hislopi*, 10 - *Parringtonia gacilis*, 11 - *Gracilisuchus stipanicicorum*, 12 - *Arizonasaurus babbitti*, 13 - *Saurosuchus galilei*, 14 - *Sphenosuchus acutus*, 15 - *Protosuchus haughtoni*, 16 - *Junggarsuchus sloani*, 17 - *Steneosaurus pictaviensis*, 18 - *Pelagosaurus typus*, 19 - *Desmatosuchus spurensis* 20 - *Postosuchus* sp., **Crocodylians:** 21 - *Tomistoma schlegelii*, 22 - *Crocodylus porosus*, 23 - *Alligator mississippiensis*, 24 - *Paleosuchus palpebrosus*, 25 - *Caiman crocodilus*, 26 - *Crocodylus acutus*, 27 - *Crocodylus intermedius*, 28 - *Crocodylus johnstoni*, 29 - *Crocodylus moreletii*, **Other avemetatarsalians:** 30 - *Teleocrater rhadinus*, **Pterosaurs:** 31 - *Allkaruen koi*, 32 - *Rhamphorhynchus muensteri*, 33 - *Anhanguera santanae*, 34 - *Ornithocheirus* sp., **Other avemetatarsalians:** 35 - *Ixalerpeton polesinensis*, 36 - *Dromomeron gregorii*, 37 - *Lewisuchus admixtus*, 38 - *Asilisaurus kongwe*, 39 - *Heterodontosaurus tucki*, 40 - *Saturnalia tupiniquim*, 41 - *Plateosaurus* sp., 42 - *Massospondylus carinatus*, 43 - *Herrerasaurus ischigualastensis*, 44 - *Gnathovorax cabreirai*, 45 - *Megapnosaurus rhodesiensis*, 46 - *Velociraptor mongoliensis*, **Birds:** 47 - *Casuarius casuarius*, 48 - *Crypturellus tataupa*, 49 - *Aythya fuligula*, 50 - *Gallus gallus*, 51 - *Columba livia*, 52 - *Grus grus*, 53 - *Phoenicopterus ruber*, 54 - *Creagrus furcatus*, 55 - *Phaethon lepturus*, 56 - *Gavia immer*, 57 - *Diomedea exulans*, 58 - *Ciconia ciconia*, 59 - *Sagittarius serpentarius*, 60 - *Aquila chrysaetos*, 61 - *Athene cunicularia*, 62 - *Sphyrapicus varius*, 63 - *Psittacus* erithacus, 64 - *Corvus corax*, **Lepidosaurs:** 65 - *Iguana iguana*, 66 - *Lacerta viridis*, 67 - *Lyriocephalus scutatus*, 68 - *Sphenodon punctatus*, 69 - *Varanus indicus*, 70 - *Amblyrhynchus cristatus*, **Turtles:** 71 - *Proganochelys quenstedti*, 72 - *Australochelys africanus*, 73 - *Eileanchelys waldmanni*, 74 - *Xinjiangchelys radiplicatoides*, 75 - *Plesiochelys planiceps*, 76 – *Portlandemys mcdowelli*, 77 - *Terrapene coahuila*, 78 - *Staurotypus salvinii*, 79 - *Psammobates tentorius*, 80 - *Trionyx triunguis*, 81 - *Chelonia mydas*, 82 - *Chelus fimbriatus*, 83 - *Podocnemis unifilis*.

FIGURE S3

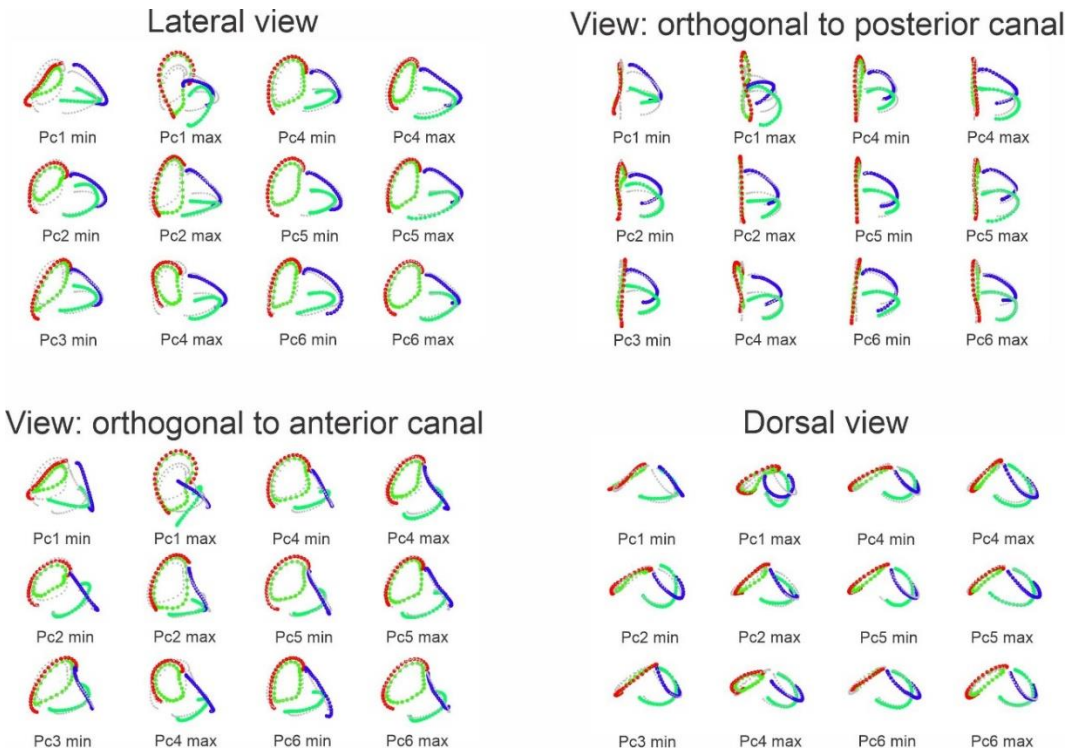

Figure S3. Landmark configurations corresponding to the mean shape (grey symbols) and deformations (colored symbols) along principal component axes PC1–PC6 from the full dataset in selected views, Related to Figure 2. Deformations correspond to the highest negative ('min') and positive ('max') score on each PC axis. Labyrinths are displayed as left labyrinths.

FIGURE S4

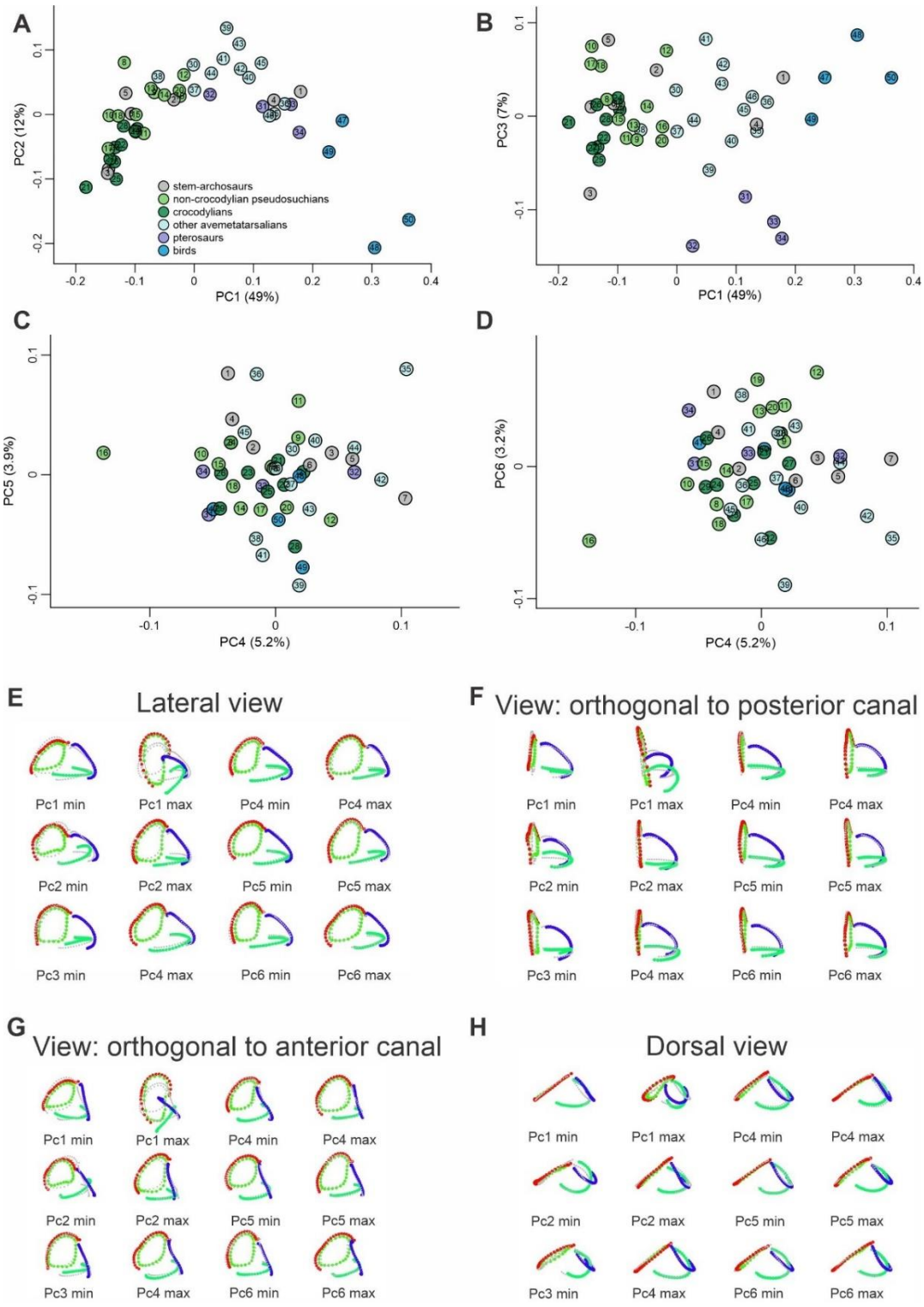

Figure S4. Plots of principal component scores from PCA of full dataset using numbers to indicate taxa (A-D) and landmark configurations corresponding to the mean shape (grey symbols) and deformations (colored symbols) along principal component axes PC1–PC6 from the full dataset in selected views (E-H), Related to Figure 2: (A) - PC1 vs. PC2; (B) - PC1 vs PC3, (C) - PC4 vs PC5; (D) - PC4 vs PC6. Numbers (1 to 50) follow those of Figure S2. Landmark configurations corresponding to the mean shape (grey symbols) and deformations (colored symbols) along principal component axes PC1–PC6 from the reduced dataset (50 taxa – see Figure S4) in selected views (E-H). Deformations correspond to the highest negative ('min') and positive ('max') score on each PC axis.

FIGURE S5

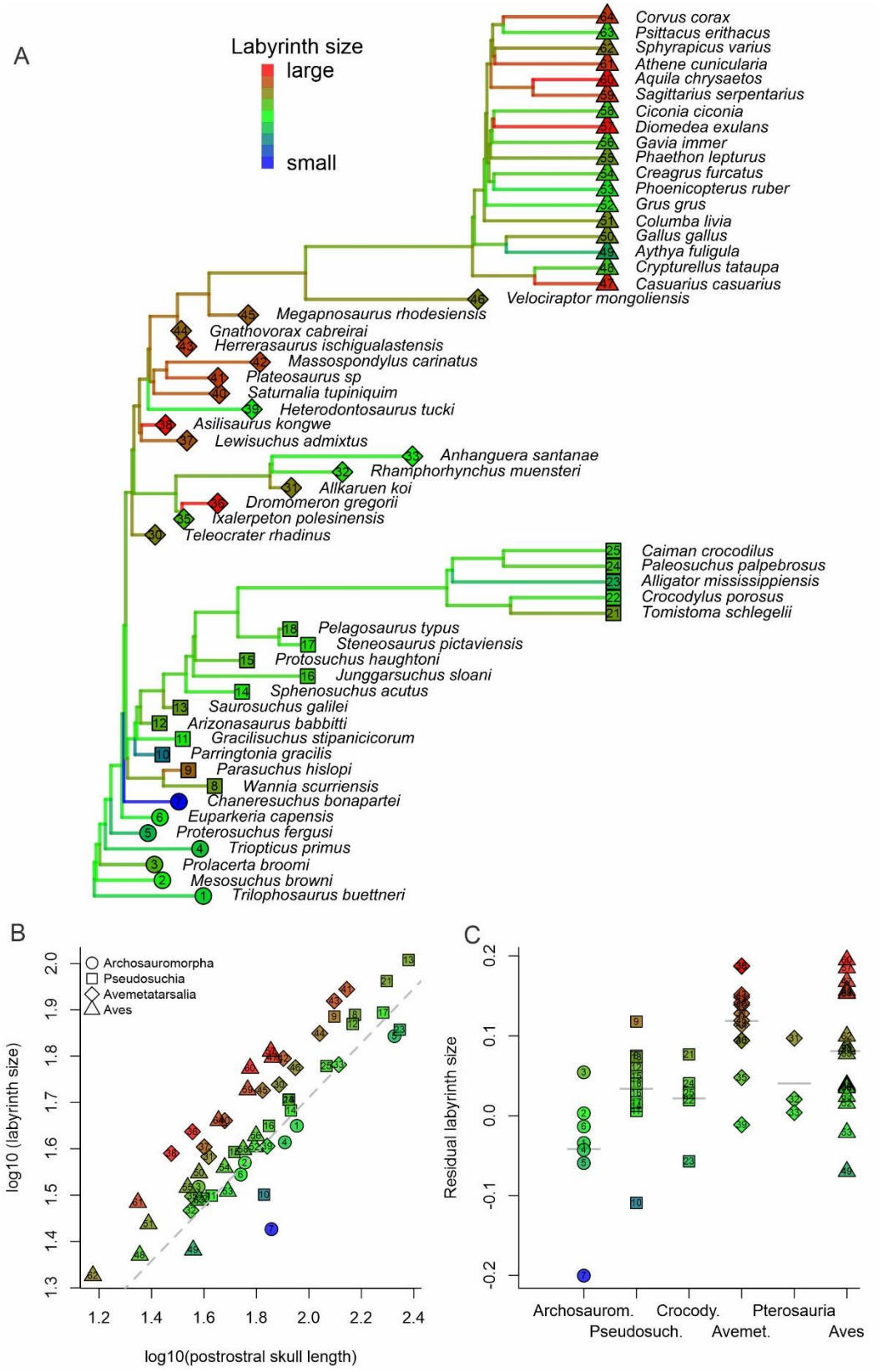

Figure S5. Semicircular canals relative size based on centroid size/postrostral length of the skull, Related to Figure 4 (A) Time-scaled archosauromorph phylogeny with branches colored according to relative labyrinth centroid size. Relative labyrinth size here is based on the residuals from our pGLS regression of labyrinth centroid size on postrostral skull length (see main text Figure 4; Table 2). Branch and tip label colors indicate relative labyrinth centroid sizes. (B) Plot of labyrinth centroid size on length of the

postrostral portion of the skull and (C) residuals of the relationship between labyrinth centroid size and length of the postrostral portion of the skull in different groups of archosauromorphs (see Main Text -Table 2). Points are colored according to residuals from the regression line. Grey horizontal lines in panel C indicate group means. Numbers indicate taxa as follows: Stem-archosaurs: 1 - *Trilophosaurus buettneri*, 2 - *Mesosuchus browni*, 3 - *Prolacerta broomi*, 4 - *Triopticus primus*, 5 - *Proterosuchus fergusi*, 6 - *Euparkeria capensis*, 7 - *Chanaresuchus bonapartei*, Non-crocodylian pseudosuchians: 8 - *Wannia scurriensis*, 9 - *Parasuchus hislopi*, 10 - *Parringtonia gacilis*, 11 - *Gracilisuchus stipanicicorum*, 12 - *Arizonasaurus babbitti*, 13 - *Saurosuchus galilei*, 14 - *Sphenosuchus acutus*, 15 - *Protosuchus haughtoni*, 16 - *Junggarsuchus sloani*, 17 - *Steneosaurus pictaviensis*, 18 - *Pelagosaurus typus*, 19 - *Desmatosuchus spurensis* 20 - *Postosuchus* sp., Crocodylians: 21 - *Tomistoma schlegelii*, 22 - *Crocodylus porosus*, 23 - *Alligator mississippiensis*, 24 - *Paleosuchus palpebrosus*, 25 - *Caiman crocodilus*, 26 - *Crocodylus acutus*, 27 - *Crocodylus intermedius*, 28 - *Crocodylus johnstoni*, 29 - *Crocodylus moreletii*, Other avemetatarsalians: 30 - *Teleocrater rhadinus*, Pterosaurs: 31 - *Allkaruen koi*, 32 - *Rhamphorhynchus muensteri*, 33 - *Anhanguera santanae*, 34 - *Ornithocheirus* sp., Other avemetatarsalians: 35 - *Ixalerpeton polesinensis*, 36 - *Dromomeron gregorii*, 37 - *Lewisuchus admixtus*, 38 - *Asilisaurus kongwe*, 39 - *Heterodontosaurus tucki*, 40 - *Saturnalia tupiniquim*, 41 - *Plateosaurus* sp., 42 - *Massospondylus carinatus*, 43 - *Herrerasaurus ischigualastensis*, 44 - *Gnathovorax cabreirai*, 45 - *Megapnosaurus rhodesiensis*, 46 - *Velociraptor mongoliensis,* Birds: 47 - *Casuarius casuarius*, 48 - *Crypturellus tataupa*, 49 - *Aythya fuligula*, 50 - *Gallus gallus*, 51 - *Columba livia,* 52 - *Grus grus,* 53 - *Phoenicopterus ruber,* 54 - *Creagrus furcatus*, 55 - *Phaethon lepturus*, 56 - *Gavia immer*, 57 - *Diomedea exulans*, 58 - *Ciconia ciconia*, 59 - *Sagittarius serpentarius*, 60 - *Aquila chrysaetos*, 61 - *Athene cunicularia*, 62 - *Sphyrapicus varius*, 63 - *Psittacus erithacus*, 64 - *Corvus corax.*

FIGURE S6

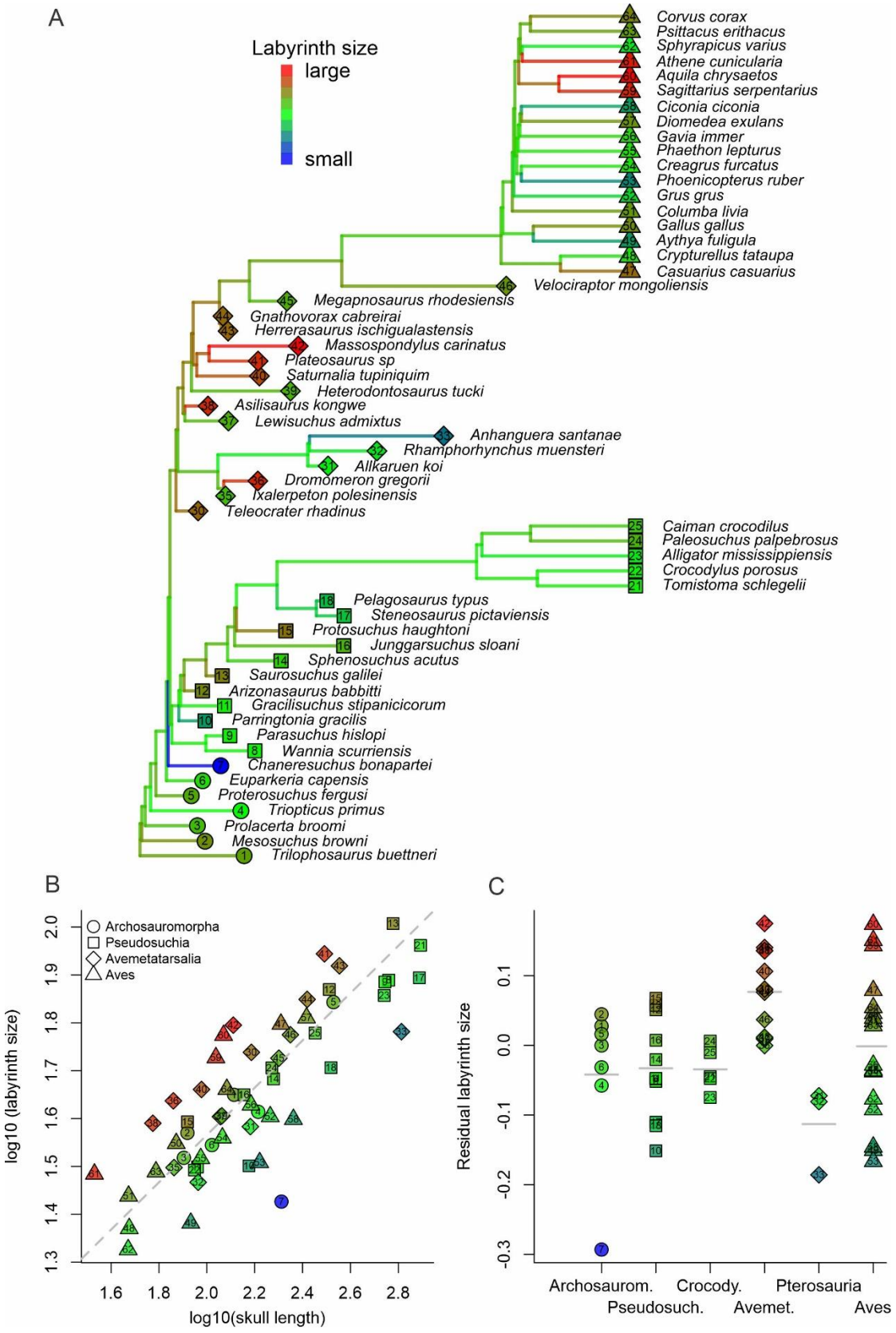

Figure S6. Semicircular canals relative size based on centroid size/skull length, Related to Figure 4. (A) Time-scaled archosauromorph phylogeny with branches colored according to relative labyrinth centroid size. Relative labyrinth size here is based on the residuals from our pGLS regression of labyrinth centroid

size on skull length (see main text Figure 4; Table 2). (B) Plot of labyrinth centroid size on skull length and (C) residuals of the relationship between labyrinth centroid size and skull length in different groups of archosauromorphs (see Main Text -Table 2). Numbers follow that of Figure S6. Points are colored according to residuals from the regression line. Grey horizontal lines in panel C indicate group means. Numbers indicate taxa as follows: Stem-archosaurs: 1 - *Trilophosaurus buettneri*, 2 - *Mesosuchus browni*, 3 - *Prolacerta broomi*, 4 - *Triopticus primus*, 5 - *Proterosuchus fergusi*, 6 - *Euparkeria capensis*, 7 - *Chanaresuchus bonapartei*, Non-crocodylian pseudosuchians: 8 - *Wannia scurriensis*, 9 - *Parasuchus hislopi*, 10 - *Parringtonia gacilis*, 11 - *Gracilisuchus stipanicicorum*, 12 - *Arizonasaurus babbitti*, 13 - *Saurosuchus galilei*, 14 - *Sphenosuchus acutus*, 15 - *Protosuchus haughtoni*, 16 - *Junggarsuchus sloani*, 17 - *Steneosaurus pictaviensis*, 18 - *Pelagosaurus typus*, 19 - *Desmatosuchus spurensis* 20 - *Postosuchus* sp., Crocodylians: 21 - *Tomistoma schlegelii*, 22 - *Crocodylus porosus*, 23 - *Alligator mississippiensis*, 24 - *Paleosuchus palpebrosus*, 25 - *Caiman crocodilus*, 26 - *Crocodylus acutus*, 27 - *Crocodylus intermedius*, 28 - *Crocodylus johnstoni*, 29 - *Crocodylus moreletii*, Other avemetatarsalians: 30 - *Teleocrater rhadinus*, Pterosaurs: 31 - *Allkaruen koi*, 32 - *Rhamphorhynchus muensteri*, 33 - *Anhanguera santanae*, 34 - *Ornithocheirus* sp., Other avemetatarsalians: 35 - *Ixalerpeton polesinensis*, 36 - *Dromomeron gregorii*, 37 - *Lewisuchus admixtus*, 38 - *Asilisaurus kongwe*, 39 - *Heterodontosaurus tucki*, 40 - *Saturnalia tupiniquim*, 41 - *Plateosaurus* sp., 42 - *Massospondylus carinatus*, 43 - *Herrerasaurus ischigualastensis*, 44 - *Gnathovorax cabreirai*, 45 - *Megapnosaurus rhodesiensis*, 46 - *Velociraptor mongoliensis,* Birds: 47 - *Casuarius casuarius*, 48 - *Crypturellus tataupa*, 49 - *Aythya fuligula*, 50 - *Gallus gallus*, 51 - *Columba livia,* 52 - *Grus grus,* 53 - *Phoenicopterus ruber,* 54 - *Creagrus furcatus*, 55 - *Phaethon lepturus*, 56 - *Gavia immer*, 57 - *Diomedea exulans*, 58 - *Ciconia ciconia*, 59 - *Sagittarius serpentarius*, 60 - *Aquila chrysaetos*, 61 - *Athene cunicularia*, 62 - *Sphyrapicus varius*, 63 - *Psittacus erithacus*, 64 - *Corvus corax.*

FIGURE S7

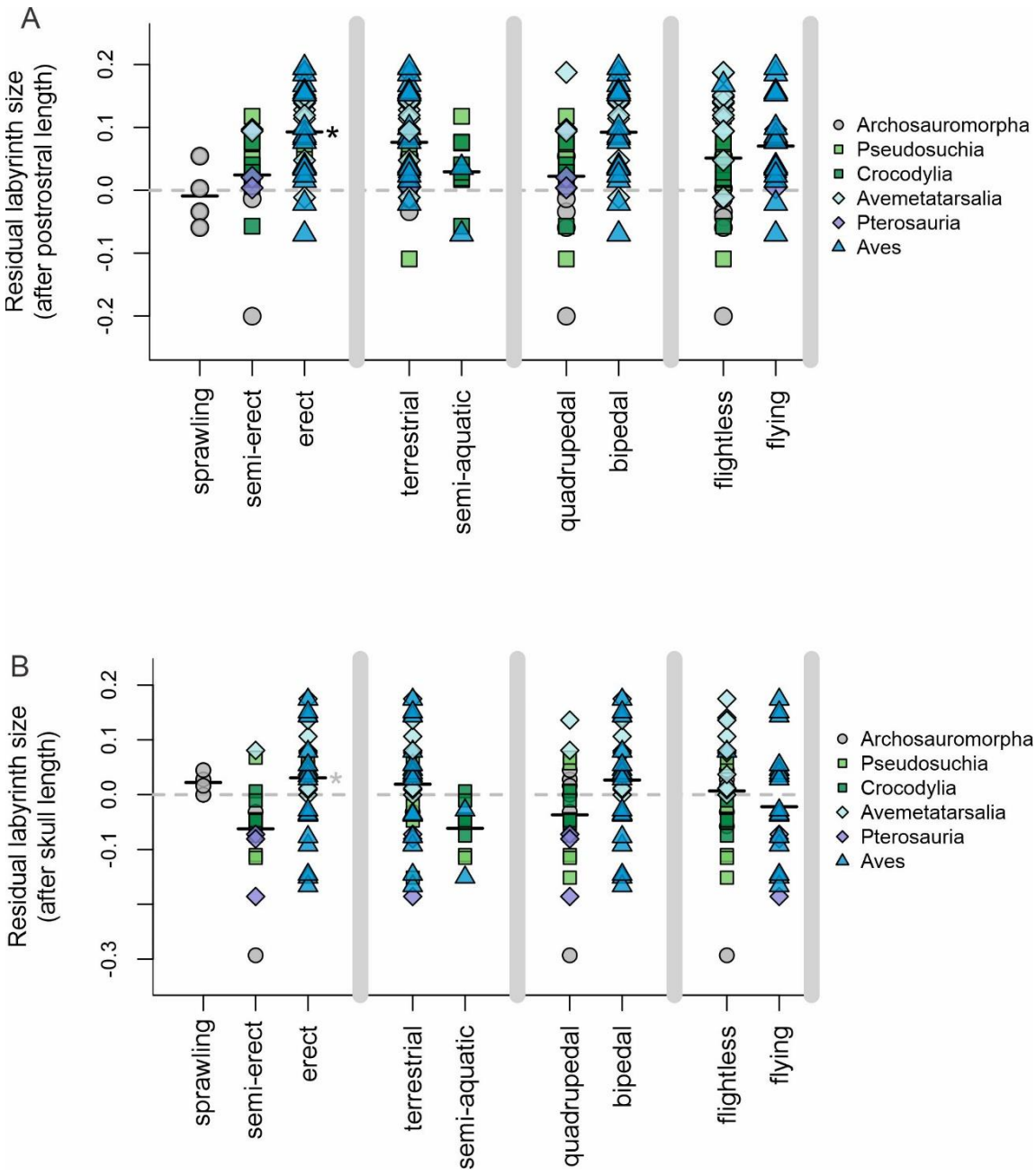

Figure S7. Pairwise comparisons of relative labyrinth centroid size variation among locomotory groups, Related to Figure 4. (A) Relative labyrinth size here is based on the residuals from our pGLS regression of labyrinth centroid size on postrostral skull length (see main text Figure 4; Table 2). Grey lines indicate groups means and the black asterisk indicates a significant difference in group means between taxa with erect limb orientations and taxa with non-erect limb orientations in our phylogenetic generalized least squares (pGLS) analyses (see Table 3). (B) Relative labyrinth size here is based on the residuals from our pGLS regression of labyrinth centroid size on full skull length (see main text Figure 4; Table 2). Grey lines indicate groups means and the grey asterisk indicates a marginally non-significant difference in group means between taxa with erect limb orientations and taxa with non-erect limb orientations in our phylogenetic generalized least squares (pGLS) analyses (see Data S1E and DATA S1F; $p = 0.066$).

Table S1.

Taxon	Lifestyle	Stance	Posture	Flight	Labyrinth Centroid size (mm)	Skull length (mm)	Postrostral length (mm)	Aspect ratio (height/width at the occiput)
Alligator mississippiensis, crocodylian	semi-aquatic	quadruped ([S1])	semi-erect	non-flier	71.96	551	222	0.45
† *Allkaruen koi*, pterosaur	terrestrial	quadruped (see Supplemental Information Text)	semi-erect	flier	38.29	152*	41.5*	NA
† *Anhanguera santanae*, pterosaur	terrestrial	quadruped ([S2])	semi-erect	flier	60.46	650*	130	1.36
Aquila chrysaetos , aves	terrestrial	biped ([S3])	erect	flier	59.42	117	59.7	0.79
† *Arizonasaurus babbitti*, pseudosuchian	terrestrial	NA	erect	non-flier	74.04	325*	147*	1.50
† *Asilisaurus kongwe*, avemetatarsalian	terrestrial	quadruped ([S4])	erect	non-flier	38.91	59.5*	29.9*	NA
Athene cunicularia, aves	terrestrial	biped ([S3])	erect	flier	30.50	34.0	22.3	0.68
Aythya fuligula, aves	semi-aquatic	biped ([S3])	erect	flier	24.08	85.7	36.2	0.96
Caiman crocodilus, crocodylian	semi-aquatic	quadruped ([S1])	semi-erect	non-flier	60.06	283	117	0.46
Casuarius casuarius, aves	terrestrial	biped ([S3])	erect	non-flier	62.72	204	72.7	0.83
† *Chaneresuchus bonapartei*, stem-archosaur	NA	quadruped ([S25])	semi-erect	non-flier	26.70	205	72.0	0.40
Ciconia ciconia, aves	terrestrial	biped ([S3])	erect	flier	39.67	230	56.2	0.84
Columba livia, aves	terrestrial	biped ([S3])	erect	flier	27.43	47.1	24.5	0.93
Corvus corax, aves	terrestrial	biped ([S3])	erect	flier	45.83	121	45.2	0.72
Creagrus furcatus, aves	terrestrial	biped ([S3])	erect	flier	36.28	116	47.7	0.85
Crocodylus porosus, crocodylian	semi-aquatic	quadruped ([S1])	semi-erect	non-flier	31.08	88.8	39.4	0.50
Crypturellus tataupa, aves	terrestrial	biped ([S3])	erect	flier	23.46	47.4	22.6	1.00
† *Desmatosuchus spurensis*, pseudosuchian	terrestrial	quadruped ([S6])	erect	non-flier	65.63	NA	NA	0.85
Diomedea exulans,aves	terrestrial	biped ([S3])	erect	flier	64.64	261	71.6	0.83
† *Dromomeron gregorii*, avemetatarsalian	terrestrial	biped ([S7])	erect	non-flier	43.35	72.5*	36.0*	NA
† *Euparkeria capensis*, stem-archosaur	terrestrial	quadruped ([S8)	semi-erect	non-flier	35.04	105*	55.0*	1.25
Gallus gallus, aves	terrestrial	biped ([S3])	erect	flier	35.33	74.5	38.1	0.94
Gavia immer aves	semi-aquatic	biped ([S3])	erect	flier	42.51	153	62.9	0.87

Table S1 (continued).

Taxon	Lifestyle	Stance	Posture	Flight	Labyrinth Centroid size (mm)	Skull length (mm)	Postrostral length (mm)	Aspect ratio (height/width at the occiput)
† *Gnathovorax cabreirai*, avemetatarsalian	terrestrial	biped ([S9])	erect	non-flier	70.62	262	110	NA
† *Gracilisuchus stipanicicorum,* pseudosuchian	terrestrial	quadruped ([S5])	semi-erect	non-flier	31.54	91.4	42.6	0.50
Grus grus, aves	terrestrial	biped ([S3])	erect	flier	40.19	184	62.0	1.29
† *Herrerasaurus ischigualastensis*, avemetatarsalian	terrestrial	biped ([S9])	erect	non-flier	82.98	358	125	0.87
† *Heterodontosaurus tucki*, avemetatarsalian	terrestrial	biped ([S10])	erect	non-flier	40.34	116	69.3	1.50
† *Ixalerpeton polesinensis*, avemetatarsalian	terrestrial	biped ([S7])	erect	non-flier	31.45	73.0*	36.0*	NA
† *Junggarsuchus sloani*, pseudosuchian	terrestrial	quadruped ([S11])	erect	non-flier	44.63	143	70.4	0.96
† *Lewisuchus admixtus*, avemetatarsalian	terrestrial	?	erect	non-flier	40.18	114*	39.9*	1.20
† *Massospondylus carinatus*, avemetatarsalian	terrestrial	biped ([S12])	erect	non-flier	62.39	129	80.0	0.77
† *Megapnosaurus rhodesiensis*, avemetatarsalian	terrestrial	biped ([S13])	erect	non-flier	53.22	200*	66.6*	1.5
† *Mesosuchus browni*, stem-archosaurs	terrestrial	quadruped ([S14])	sprawling	non-flier	37.17	83.0	57.0	0.50
† *Ornithocheirus* sp, pterosaur	terrestrial	quadruped ([S15])	semi-erect	flier	50.33	NA	NA	NA
Paleosuchus palpebrosus, crocodylian	semi-aquatic	quadruped ([S1])	semi-erect	non-flier	50.79	187	83.7	0.47
† *Parasuchus hislopi*, pseudosuchian	semi-aquatic	quadruped ([S16])	semi-erect	non-flier	76.80	555*	125	0.55
† *Parringtonia gracilis*, pseudosuchian	terrestrial	quadruped ([S17])	NA	non-flier	31.71	150*	67.5*	0.50
† *Pelagosaurus typus*, pseudosuchian	semi-aquatic	quadruped ([S18])	semi-erect	non-flier	50.86	330*	84.0	0.48
Phaethon lepturus,aves	terrestrial	biped ([S3])	erect	flier	32.86	94.3	34.5	0.94
Phoenicopterus ruber, aves	terrestrial	biped ([S3])	erect	flier	32.22	166	49.1	0.96

Table S1 (continued).

Taxon	Lifestyle	Stance	Posture	Flight	Labyrinth Centroid size (mm)	Skull length (mm)	Postrostral length (mm)	Aspect ratio (height/width at the occiput)
† *Plateosaurus* sp., avemetatarsalian	terrestrial	biped ([S12])	erect	non-flier	87.92	310	139	1.50
† *Postosuchus* sp., pseudosuchian	terrestrial	biped ([S9])	erect	non-flier	88.81	NA	NA	1.03
† *Prolacerta broomi*, stem-archosaur	terrestrial	quadruped ([S20])	sprawling	non-flier	32.96	80.2*	38.0	0.64
† *Proterosuchus fergusi*, stem-archosaur	NA	quadruped ([S21])	sprawling	non-flier	69.68	338	212	0.37
† *Protosuchus haughtoni*, pseudosuchian	terrestrial	quadruped ([S22])	semi-erect	non-flier	39.19	83.0	52.0	0.66
Psittacus erithacus, aves	terrestrial	biped ([S3])	erect	flier	30.82	61.3	38.2	0.75
† *Rhamphorhynchus muensteri*, pterosaur	terrestrial	quadruped ([S23])	semi-erect	flier	29.30	92.0	35.5	1.90
Sagittarius serpentarius, aves	terrestrial	biped ([S3])	erect	flier	35.12	120	50.6	0.79
† *Saturnalia tupiniquim*, avemetatarsalian	terrestrial	biped ([S12])	erect	non-flier	45.79	95.0*	47.7*	1.15
† *Saurosuchus galilei*, pseudosuchian	terrestrial	quadruped ([S24])	erect	non-flier	101.7	600	240	0.87
† *Sphenosuchus acutus*, pseudosuchian	terrestrial	NA	NA	non-flier	48.18	190*	85.5*	0.77
Sphyrapicus varius, aves	terrestrial	biped ([S4])	erect	flier	21.20	46.9	15.0	0.82
† *Steneosaurus pictaviensis*, pseudosuchian	semi-aquatic	quadruped ([S18])	semi-erect	non-flier	78.34	772	192	0.31
Teleocrater rhadinus, avemetatarsalian	terrestrial	quadruped ([S25])	semi-erect	non-flier	54.74	153*	77.1*	NA
Tomistoma schlegelii, crocodylian	semi-aquatic	quadruped ([S1])	semi-erect	non-flier	91.58	781	198	0.49
† *Trilophosaurus buettneri*, stem-archosaur	terrestrial	quadruped ([S26])	sprawling	non-flier	44.63	130*	90.0*	1.05
† *Triopticus primus*, stem-archosaur	NA	NA	NA	non-flier	41.12	164*	81.0	NA
† *Velociraptor mongoliensis*	terrestrial	Biped	erect	non-flier	59.57	49.3	88.9	1.10
† *Wannia scurriensis*, pseudosuchian	semi-aquatic	quadruped ([S16])	semi-erect	non-flier	77.48	575*	150	0.55

Table S1. Locomotor categories and relevant cranial and labyrinth measurements, Related to STAR Methods.

Additional references

S1. Grigg G, Kirshner D. 2015 Biology and evolution of crocodylians. Melbourne, Australia: CSIRO Publishing.

S2. Costa FR, Rocha-Barbosa O, Kellner AWA. 2014. A biomechanical approach on the optimal stance of Anhanguera piscator (Pterodactyloidea) and its implications for pterosaur gait on land. *Historical Biology,* 26(5), 582-590.

S3. Gatesy SM, Dial KP. 1996. Locomotor modules and the evolution of avian flight. *Evolution,* 50, 331-340.

S4. Nesbitt SJ, Sidor CA, Irmis RB, Angielczyk KD, Smith RM, Tsuji LA. 2010. Ecologically distinct dinosaurian sister group shows early diversification of Ornithodira. Nature. 464: 95-8.

S5. Arcucci AB. 1988. Locomotor structures in the Middle Triassic archosaurs from Los Chañares (La Rioja, Argentina). Historical Biology, 3, 85-95.

S6. Small BJ. 1985. The Triassic Thecodontian Reptile *Desmatosuchus:* Osteology and Relationships. *Master Thesis Texas Tech University*.

S7. Ezcurra MD, Nesbitt SJ, Bronzati M, Dalla-Vechia F, Agnolin FL, Benson RBJ, Brissón Egli F, Cabreira SF, Evers SW, Gentil AR, Irmis RB, Martinelli AG, Novas FE, Roberto-da-Silva L, Smith ND, Stocker MR, Turner AH, Langer MC. In press. Enigmatic dinosaur precursors bridge the gap to the origin of Pterosauria. *Nature*

S8. Sookias RB, Butler RJ. 2013. Euparkeriidae. *Geological Society, London, Special Publications*. 379, 35–48

S9. Pacheco C, Müller RT, Langer M, Pretto FA, Kerber L, Dias da Silva S. 2019. Gnathovorax cabreirai: a new early dinosaur and the origin and initial radiation of predatory dinosaurs. PeerJ 7:e7963

S10. Weishampel DB, Witmer LM. 1990. Heterodontosauridae. In Weishampel DB, Dodson P, Osmólska H. (eds.). The Dinosauria. University of California Press. pp. 486–497

S11. Clark JM, Xu X, Forster CA, Wang Y. 2004. A Middle Jurassic 'sphenosuchian' from China and the origin of the crocodylian skull. *Nature*. 430, 1021–1024

S12. McPhee BW, Benson RBJ, Botha-Brink J, Bordy EM, Choiniere JN. 2018. A Giant Dinosaur from the Earliest Jurassic of South Africa and the Transition to Quadrupedality in Early Sauropodomorphs. *Current Biology,* 28, 3143-3151.

S13. Raath MA. 1969. A new Coelurosaurian dinosaur from the Forest Sandstone of Rhodesia. *Arnoldia Rhodesia*, 4(28), 1-25.

S14. Dilkes DW. 1997. The Early Triassic rhynchosaur *Mesosuchus browni* and the interrelationships of basal archosauromorph reptiles. *Philosophical Transactions of the Royal Society B: Biological Sciences*, 353, 501–541.

S15. Witton MP, Habib MB. 2010. On the Size and Flight Diversity of Giant Pterosaurs, the Use of Birds as Pterosaur Analogues and Comments on Pterosaur Flightlessness. *PlosOne,* 5, e13982.

S16. Stocker MR, Butler RJ. 2013. Phytosauria. Geological Society London Special Publications, 379, 91-117.

S17. Nesbitt SJ, Stocker MR, Parker WG, Wood TA, Sidor CA, Angielczyk D. 2018. The braincase and endocast of Parringtonia gracilis, a Middle Triassic suchian (Arhocusaur: Pseudosuchia). Journal of Vertebrate Palaeontology, 37:sup1, 122–141.

S18. Westphal F. 1962. Die krokodilier des Deutschen und Englischen oberen Lias. *Palaeontographica A* 116, 23–11.

S19. Weinbaum J. 2013. Postcranial skeleton of *Postosuchus kirkpatricki* (Archosauria: Paracrocodylomorpha), from the Upper Triassic of the United States. *Geological Society London Special Publications* 379(1), 525-553

S20. Gow CE. 1975. The morphology and the relationships of *Youngina capensis* Broom and *Prolacerta broomi* Parrington. *Palaeont. Afr.* 18, 89-131.

S21.Cruickshank ARI. 1972. The proterosuchian thecodonts. In Joysey KA and Kemp TS (editors), Studies in vertebrate evolution, 89–119. Edinburgh: Oliver and Boyd.

S22. Colbert EH, Mook CG. 1951. The ancestral crocodilian *Protosuchus. Bulletin of the American Museum of Natural History,* 97, 143-182.

S23. Witton MP. 2015. Were early pterosaurs inept terrestrial locomotors? PeerJ 3:e1018

S24. Sill WD, 1974. The anatomy of *Saurosuchus galilei* and the relationships of the rauisuchid thecodonts. *Harvard Museum of Comparative Zoology, Bulletin*, 146(7), 317362.

S25. Nesbitt SJ, Butler RJ, Ezcurra MD, Barrett PM, Stocker MR. et al. 2017. The earliest bird-line archosaurs and the assembly of the dinosaur body plan. Nature, 544, 484–487.

S26. Spielmann JA, Heckert AB, Lucas SG. 2008. The Late Triassic achosauromorph Trilophosaurus as an arboreal climber. Riv. Ital. Paleontol. S. 111, 395-412.

ADDITIONAL INFORMATION ON SPECIMENS, INCLUDING COLLECTION NUMBER, PHYLOGENETIC POSITION, AND THE ORIGINAL SOURCE OF THE 3D MODEL OF THE SEMICIRCULAR CANALS FOR EACH TAXON USED IN THE STUDY:

TITLE: Deep evolutionary diversification of semicircular canals in archosaurs

Authors

Mario Bronzati[a,1,*], Roger B. J. Benson[b,c,1,*], Serjoscha W. Evers[b,d], Martín D. Ezcurra[e,f], Sergio F. Cabreira[g], Jonah Choiniere[c], Kathleen N. Dollman[c], Ariana Paulina-Carabajal[h], Viktor J. Radermacher[c], Lucio Roberto-da-Silva[i], Gabriela Sobral[j], Michelle R. Stocker[k], Lawrence M. Witmer[l], Max C. Langer[a], Sterling J. Nesbitt[k,*]

[a]Departamento de Biologia, Universidade de São Paulo, Av. Bandeirantes 1900, Ribeirão Preto-SP, 14040-091, Brazil; [b]Department of Earth Sciences, University of Oxford, South Parks Road, OX13AN, Oxford, UK; [c]Evolutionary Studies Institute, University of the Witwatersrand, Braamfontein, Private Bag 3, Johannesburg, WITS2050, South Africa; [d]Department of Geosciences, University of Fribourg, Chemin du Musée 4, CH-1700 Fribourg, Switzerland; [e]Sección Paleontología de Vertebrados, CONICET–Museo Argentino de Ciencias Naturales "Bernardino Rivadavia", Ángel Gallardo 470, C1405DJR, Buenos Aires, Argentina; [f]School of Geography, Earth and Environmental Sciences, University of Birmingham, Edgbaston, B15 2TT, Birmingham, UK; [g]Avenida Antônio Bozzetto 305, Faxinal do Soturno-RS, 97220-000, Brazil; [h]Instituto de Investigaciones en Biodiversidad y Medioambiente (INIBIOMA), CONICET-Universidad Nacional del Comahue, Quintral 1250 (8400), San Carlos de Bariloche, Argentina; [i]Rua Venâncio Trindade 810, Cachoeira do Sul-RS, 96506-290, Brazil; [j]Staatliches Museum für Naturkunde Stuttgart, Rosenstein 1, Suttgart, 70191, Germany; [k]Department of Geosciences, Virginia Tech, 926 West Campus Drive, Blacksburg, VA 24061, USA; [l]Department of Biomedical Science, Heritage College of Osteopathic Medicine, Ohio University, Athens, Ohio 45701, USA.

[1] these authors contributed equally

* Correspondence: Mario Bronzati (lead contact) – email: mariobronzati@gmail.com, TEL: +55 16 33154965; Roger B. J. Benson – email: roger.benson@earth.ox.ac.uk, TEL: +44 1865 272076; Sterling J. Nesbitt: sjn2104@vt.edu, Tel: +1 540 231 6330.

1. Institutional Abbreviations

AM – Albany Museum, Grahamstown, South Africa; **AMNH** – American Museum of Natural History, New York, USA; **BP** – Bernard Price Institute, Johannesburg, South Africa; **BSPG or SNSN-BSPG** – Bayerische Staatssammlung für Paläontologie und Geologie, Munich, Germany; **CAMSM** – Sedgwick Museum, University of Cambridge, UK; **CM** – Carnegie Museum of Natural History, Pittsburgh, Pennsylvania, USA; **CAPPA/UFSM** – Centro de Apoio à Pesquisa Paleontológica da Quarta Colônia, Universidade Federal de Santa Maria, São João do Polêsine, Brazil; **CRILAR-Pv** – Centro Regional de Investigaciones Científicas y Transferencia Tecnológica de La Rioja, Paleontología de Vertebrados, Anillaco, Argentina; **FMNH** – Field Museum of Natural History, Chicago, USA; **ISIR** – Geology Museum, Indian Statistical Institute, Reptiles, Calcutta, India; **IVPP** – Institute of Vertebrate Paleontology and Paleoanthropology, Beijing, China; **LPP** – Institut de paléoprimatologie, paléontologie, humaine; évolution et paléoenvironnements Université de Poitiers, Poitiers, France; **MB.R**. or **MB** – Museum für Naturkunde Berlin, Berlin, Germany; **MCP** – Museu de Ciências e Tecnologia da PUCRS, Porto Alegre, Brazil; **MCZ** – Museum of Comparative Zoology, Harvard University, Cambridge, Massachusetts, USA; **MPEF** – Museo Paleontológico Edigio Feruglio, Trelew, Argentina; **MSM** – Mesa Southwest Museum, Mesa, Arizona, USA; **NHMUK** – Natural History Museum, London, United Kingdom; **NMS** – National Museums Scotland, Edinburgh, Scotland; **NMT** – National Museum of Tanzania, Dar es Salaam, Tanzania; **OUMNH** – Oxford University Museum of Natural History, Oxford, United Kingdom; **OUVC** – Ohio University Vertebrate Collections, Athens, Ohio; **PCHP** – Chelonian Research Institute/Peter C.H. Pritchard, Oviedo, USA; **PVSJ** – División de Paleontología de Vertebrados del Museo de Ciencias Naturales y Universidad Nacional de San Juan, San Juan, Argentina; **QG** – Natural History Museum of Zimbabwe, Bulawayo, Zimbabwe; **SAM** – Iziko South African Museum, Cape Town, South Africa; **SMF** – Forschungsinstitut und Natur-Museum Senckenberg, Frankfurt-am-Main, Germany; **TMM** – Texas Memorial Museum, Austin, USA; **TTU** – Texas Tech University, Lubbock, USA; **ULBRA** – Museu de Ciências Naturais, Universidade Luterana do Brasil, Canoas, Brazil; **UCMP** – University of California Museum of Paleontology, Berkeley, California, USA; **UMM** – Museum of Paleontology, University of Michigan, Ann Arbor, Michigan, USA; **UMMZ** – University of Michigan Museum of Zoology, University of Michigan, Ann Arbor, Michigan, USA; **USNM** – National Museum of Natural History, Smithsonian Institution, Washington D.C., USA.

2. Dataset

Information including collection number, phylogenetic position, and the original source of the 3D model of the semicircular canals for each taxon are provided below; '†' before species name indicates it is an extinct taxon.

Alligator mississippiensis USNM 211233, Crocodylia, Scanned at OhioHealth O'Bleness Hospital (Athens, USA) - 3D model generated by L.M.W; † ***Allkaruen koi*** MPEF-PV 3613, Pterosauria, Codorniú et al. [S1]; ***Amblyrhynchus cristatus*** OUMNH 11616, Lepidosauria, Scanned at University of Bristol, School of Earth Sciences - 3D model generated by S.W.E.; † ***Anhanguera santanae*** AMNH 25555, Pterosauria, Witmer et al. [S2]; ***Aquila chrysaetos*** NMS Z.1997.29.1, Aves, Benson et al. [S3]; † ***Arizonasaurus babbitti*** MSM P4590, Pseudosuchia, Scanned at Duke University's Shared Materials Instrumentation Facility (Durham, USA) - 3D model generated by M.B.; ***Athene cunicularia*** NHMUK ZOO S/1986.75.13 – Aves, Benson et al. [S3]; † ***Asilisaurus kongwe*** NMT RB486, Avemetatarsalia, Scanned at Duke University's Shared Materials Instrumentation Facility (Durham, USA) - 3D model generated by M.B.; † ***Australochelys africanus*** BP/1/4933, Testudinata, Scanned at the University of the Witwatersrand microfocus CT facility (Johannesburg, South Africa) - 3D model generated by

S.W.E.; ***Aythya fuligula*** NHMUK S1987.27.1, Aves, Benson et al. [S3]; ***Caiman crocodilus*** FMNH 73438, Crocodylia, Scanned at OhioHealth O'Bleness Hospital (Athens, USA) - 3D model generated by L.M.W.; ***Casuarius casuarius*** NHMUK 1939.12.9.964, Aves, Benson et al. [S3]; † ***Chanaresuchus bonapartei*** MCZ 4039, stem-archosaur, Stocker et al. [S4]; ***Chelonia mydas*** NHMUK 1969.776, Testudinata, Evers [S5]; ***Chelus fimbriatus*** NHMUK 81.9.27.4, Testudinata, Evers [S5]; ***Ciconia nigra*** NHMUK S/1952.1.103, Aves, Benson et al. [S3]; ***Columba livia*** NMS Unregistered, Aves, Benson et al. [S3]; ***Corvus corax*** NHMUK S1979.66.160, Aves, Benson et al. [S3]; ***Creagrus furcatus*** NHMUK S/1967.19.6, Aves, Benson et al. [S3]; ***Crocodylus acutus*** FMNH 59071, Crocodylia, Scanned at OhioHealth O'Bleness Hospital (Athens, USA) - 3D model generated by L.M.W.; ***Crocodylus intermedius*** FMNH 75662, Crocodylia, Scanned at OhioHealth O'Bleness Hospital (Athens, USA) - 3D model generated by L.M.W.; ***Crocodylus johnstoni*** OUVC 10425, Crocodylia, Scanned at OhioHealth O'Bleness Hospital (Athens, USA) - 3D model generated by L.M.W.; ***Crocodylus moreletii*** TMM M4980, Crocodylia, Scanned at OhioHealth O'Bleness Hospital (Athens, USA) - 3D model generated by L.M.W.; ***Crocodylus porosus*** OUVC 10899, Crocodylia, Scanned at OhioHealth O'Bleness Hospital (Athens, USA) - 3D model generated by L.M.W.; ***Crypturellus tataupa*** UMMZ 201948, Aves, Scanned at University of Michigan CT Earth and Environmental Sciences; † ***Desmatosuchus spurensis*** UCMP 27410, Pseudosuchia, Stocker et al. [S4]; ***Diomedea exulans*** NMS Z.1921.143.1630, Aves, Benson et al. [S3]; † ***Dromomeron gregorii*** TMM 31100-1334, Avemetatarsalia, Scanned at the University of Texas High-Resolution X-ray CT Facility (Austin, USA) - 3D model generated by M.B.; † ***Eileanchelys waldmanni*** NMS G 2004 31 15, Testudinata, Scanned at University of Bristol - 3D model generated by S.W.E.; † ***Euparkeria capensis*** SAM-PK-7696, stem-archosaur, Scanned at the Museum für Naturkunde (Berlin, Germany) - 3D model generated by S.W.E.; ***Gallus gallus*** NMS Z1931.43, Aves, Benson et al. [S3]; ***Gavia immer*** NMS Unregistered, Aves, Benson et al. [S3]; † ***Gnathovorax cabreirai*** CAPPA-UFSM 0009, Dinosauria, Pacheco et al. [S6]; † ***Gracilisuchus stipanicicorum*** MCZ 4117, Pseudosuchia, Stocker et al. [S4]; ***Grus grus*** NMS Z.1904.80.6, Aves, Benson et al. [S3]; † ***Herrerasaurus ischigualastensis*** MCZ 7063, Dinosauria, Stocker et al. [S4]; † ***Heterodontosaurus tucki*** AM 4766, Dinosauria, Scanned at the European Synchrotron Radiation Facility (Grenoble, France) - 3D model generated by V.R.; ***Iguana iguana*** OUMNH 21548, Lepidosauria, Scanned at University of Bristol, School of Earth Sciences – 3D model generated by S.W.E.; † ***Ixalerpeton polesinensis*** ULBRA PVT059, Avemetatarsalia, Scanned at the Centro para Documentacão da Biodiversidade (Ribeirão Preto, Brazil) - 3D model generated by M.B.; † ***Junggarsuchus sloani*** IVPP V14010, Pseudosuchia, Schwab et al. [S7]; ***Lacerta viridis*** OUMNH 15055, Lepidosauria, Scanned at University of Bristol, School of Earth Sciences – 3D model generated by S.W.E.; † ***Lewisuchus admixtus*** CRILAR-Pv 552, Avemetatarsalia, Ezcurra et al. [S8]; ***Lyriocephalus scutatus*** OUMNH 1298, Lepidosauria, Scanned at University of Bristol, School of Earth Sciences – 3D model generated by S.W.E.; † ***Massospondylus carinatus*** BP /1/ 4779, Dinosauria, Sereno et al. [S9]; †

Megapnosaurus rhodesiensis QG 195, Dinosauria, Scanned at Duke University's Shared Materials Instrumentation Facility (Durham, USA) - 3D model generated by M.B.; † ***Mesosuchus browni*** SAM-PK-6536, stem-archosaur, Sobral and Müller [S10] - 3D model generated by S.W.E.; † ***Ornithocheirus* sp.** CAMSM SMC B 54405, Pterosauria, Scanned at Ohio University MicroCT Scanning Facility (Athens, USA) - 3D model generated by L.M.W.; ***Paleosuchus palpebrosus*** FMNH 69867, Crocodylia, Scanned at OhioHealth O'Bleness Hospital (Athens, USA) - 3D model generated by L.M.W.; † ***Parasuchus hislopi*** ISIR 44, Pseudosuchia, Stocker et al. [S4]; † ***Parringtonia gracilis*** NMT RB426, Pseudosuchia, Nesbitt et al. [S11]; † ***Pelagosaurus typus*** NHMUK PVOR32599, Pseudosuchia, Schwab et al. [S7]; ***Phaethon lepturus*** NHMUK ZOO 1884.2.29.10, Aves, Benson et al. [S3]; ***Phoenicopterus ruber*** NMS Z.2000.193.1, Aves, Benson et al. [S3]; † ***Plateosaurus* sp**. MBR 1937, Dinosauria, 3D model generated by L.M.W.; † ***Plesiochelys planiceps*** OUMNH.J.1582, Testudinata, Evers & Benson [S12]; ***Podocnemis unifilis*** FMNH 45657, Testudinata, Evers [S5]; † ***Portlandemys mcdowelli*** NHMUK R2914, Testudinata, Scanned at Cambridge Biotomography Center - 3D model generated by S.W.E.; † ***Postosuchus* sp.** UMM P7473, Pseudosuchia, Stocker et al. [S4]; † ***Proganochelys quenstedti*** MB 1910.45.2, Testudinata, Lautenschlager et al. [S13]; † ***Prolacerta broomi*** BP/1/5375, stem-archosaur, Scanned at the University of the Witwatersrand microfocus CT facility (Johannesburg, South Africa) - 3D model generated by S.W.E.; † ***Proterosuchus fergusi*** SNSB-BSPG 1934 VIII 514, stem-archosaur, Brown et al. [S14]; † ***Protosuchus haughtoni*** BP/1/4746, Pseudosuchia, Scanned at the University of the Witwatersrand microfocus CT facility (Johannesburg, South Africa) - 3D model generated by K.D.; ***Psammobates tentorius*** SMF 57142, Testudinata, Scanned at Senckenberg Frankfurt - 3D model generated by S.W.E., ***Psittacus erithacus*** NHMUK ZOO S/1973.66.109, Aves, Benson et al. [S3]; † ***Rhamphorhynchus muensteri*** CM 11434, Pterosauria, Witmer et al. [S2]; ***Sagittarius serpentarius*** NHMUK S/2016.25.1, Aves, Benson et al. [S3]; † ***Saturnalia tupiniquim*** MCP 3845 PV, Dinosauria, Bronzati et al. [S15]; † ***Saurosuchus galilei*** PVSJ 32, Pseudosuchia, Scanned at OhioHealth O'Bleness Hospital (Athens, USA) - 3D model generated by L.M.W.; ***Sphenodon punctatus*** OUMNH 908, Lepidosauria, Scanned at University of Bristol, School of Earth Sciences – 3D model generated by S.W.E.; † ***Sphenosuchus acutus*** SAM PK 3014, Pseudosuchia, Scanned at Stellenbosch CT scanning facility (Stellenbosch, South Africa; du Plessis et al. [S16]) - 3D model generated by K.D.; ***Sphyrapicus varius*** NHMUK S/2001.25.6, Aves, Scanned at University of Bristol, School of Earth Sciences; ***Staurotypus salvinii*** NHMUK 1879.1.7.5, Testudinata, Evers [S5]; † ***Steneosaurus pictaviensis*** LPP M35, Pseudosuchia, Schwab et al. [S7]; † ***Teleocrater rhadinus*** NMT RB491, Avemetatarsalia, Scanned at Duke University's Shared Materials Instrumentation Facility (Durham, USA) - 3D model generated by M.B.; ***Terrapene coahuila*** FMNH 47372, Testudinata, Evers [S5]; ***Tomistoma schlegelii*** USNM 211322, Crocodylia, Scanned at OhioHealth O'Bleness Hospital (Athens, USA) - 3D model generated by L.M.W.; † ***Trilophosaurus buettneri*** TMM 31100 443, stem-archosaur, Scanned

at Duke University's Shared Materials Instrumentation Facility (Durham, USA) - 3D model generated by M.B.; ***Trionyx triunguis*** PCHP 4559, Testudinata, *http://digimorph.org/specimens/Trionyx_triunguis/* – 3D model generated by S.W.E.; † ***Triopticus primus*** TMM 31100, stem-archosaur, Stocker et al. [S4]; ***Varanus indicus*** AMNH 58389, Lepidosauria, Scanned at University of Bristol, School of Earth Sciences – 3D model generated by S.W.E.; † ***Velociraptor mongoliensis*** IGM 100/982, Avemetatarsalia, Logan King [S17]; † ***Wannia scurriensis*** TTU P00539, Pseudosuchia, Lessner & Stocker [S18]; † ***Xinjiangchelys radiplicatoides*** IVPP V9539, Testudinata, Brinkman et al. [S19] - 3D model generated by S.W.E.

3. References

S1. Codorniú L, Paulina Carabajal A, Pol D, Unwin D, Rauhut OWM. 2016. A Jurassic pterosaur from Patagonia and the origin of the pterodactyloid neurocranium. PeerJ, 4:e2311

S2. Witmer LM, Chatterjee S, Franzosa J, Rowe T. 2003. Neuroanatomy of the flying reptiles and implications for flight, posture and behaviour. Nature, 425, 950-953.

S3. Benson RBJ, Starmer-Jones E, Close RA, Walsh SA. 2017. Comparative analysis of vestibular ecomorphology of birds. Journal of Anatomy, 231, 990-1018. 3D models available on Morphosource: http://morphosource.org/Detail/ProjectDe tail/Show/project_id/377

S4. Stocker MD, Nesbitt SJ, Criswell KE, Parker WG, Witmer LM, et al. 2016. A Dome-Headed Stem Archosaur Exemplifies Convergence among Dinosaurs and Their Distant Relatives Current Biology, 26,2674-2680.

S5. Evers S. 2019. Project: Evers. 2019. CT scans of extant turtle skulls - https://www.morphosource.org/Detail/ProjectDetail/Show/project_id/769

S6. Pacheco C, Müller RT, Langer M, Pretto FA, Kerber L, Dias da Silva S. 2019. Gnathovorax cabreirai: a new early dinosaur and the origin and initial radiation of predatory dinosaurs. PeerJ 7:e7963

S7. Schwab JA, Young MT, Neenan JM, Walsh SA, Witmer LW. et al. 2020. Inner ear sensory system changes as extinct crocodylomorphs transitioned from land to water. PNAS . 3D models available on Morphsource: https://www.morphosource.org/Detail/ProjectDetail/Show/project_id/952

S8. Ezcurra MD, Sterling SJ, Fiorelli LE, Desojo JB. 2020. New specimen sheds light on the anatomy and taxonomy of the early Late Triassic dinosauriforms from the Chañares Formation, NW Argentina. The Anatomical Record, 303(5), 1393-1498.

S9. Sereno PC, Wilson JA, Witmer LM, Whitlock JA, Maga A, Ide O, et al. 2007. Structural Extremes in a Cretaceous Dinosaur. PLoS ONE, 2(11), e1230.

S10. Sobral G, Müller J. 2019. The braincase of Mesosuchus browni (Reptilia, Archosauromorpha) with information on the inner ear and description of a pneumatic sinus. PeerJ 7:e6798

S11. Nesbitt SJ, Stocker MR, Parker WG, Wood TA, Sidor CA, Angielczyk D. 2018. The braincase and endocast of Parringtonia gracilis, a Middle Triassic suchian (Arhocusaur: Pseudosuchia). Journal of Vertebrate Palaeontology, 37:sup1, 122–141.

S12, Evers S. Benson RBJ. 2018. Project: Evers & Benson 2018, Turtle CT Data and 3D Models - https://www.morphosource.org/Detail/ProjectDetail/Show/project_id/462

S13. Lautenschlager S, Ferreira GS, Werneburg I. 2018. Sensory Evolution and Ecology of Early Turtles Revealed by Digital Endocranial Reconstructions. *Frontiers in Ecology and Evolution,* 6, 7.

S14. Brown EE, Butler RJ, Ezcurra MD, Bhullar B-AS, Lautenschlager S. 2019. Endocranial anatomy and life habits of the Early Triassic archosauriform Proterosuchus fergusi. Palaeontology, 63(2), 255-282.

S15. Bronzati M, Rauhut OWM, Bittencourt JS, Langer MC. 2017. Endocast of the Late Triassic (Carnian) dinosaur Saturnalia tupiniquim: implications for the evolution of brain tissue in Sauropodomorpha. Scientific Reports, 7, 11931.

S16. du Plessis A, le Roux SG, Guelpa A. 2016. The CT Scanner Facility at Stellenbosch University: An open access X-ray computed tomography laboratory. Nuclear Instruments and Methods in Physics Research Section B: Beam Interactions with Materials and Atoms, 384, 42-49.

S17. Logan King J, Sipla JS, Georgi JA, Balanoff AM, Neenan JM. 2020. The endocranium and trophic ecology of *Velociraptor mongoliensis*. *Journal of Anatomy,* 237(5), 861-869.

S18. Lessner EJ, Stocker MR. 2017. Archosauriform endocranial morphology and osteological evidence for semiaquatic sensory adaptations in phytosaurs. *Journal of Anatomy,* 231, 655-664.

S19. Brinkman DB, Eberth D, Clark J, Xu X, Wu X.-C. 2013. Turtles from the Jurassic Shishugou formation of the Junggar Basin, People's Republic of China, and the basicranial region of basal eucryptodires. In Brinkman DB, Holroyd PA, Gardner JD (eds) Morphology and Evolution of Turtles, Springer. pp. 147-172

Click here to access/download

Supplemental Videos and Spreadsheets

DATA S1.xlsx

ZIP File

Click here to access/download

ZIP File

Archosaur labyrinths data and scripts.zip